UNIVERSITÀ DEGLI STUDI DI MILANO

Department of Clinical Sciences and Community Health

Doctoral Program in Public Health Sciences

XXXVII Cycle

MEDS-25/B – Occupational Medicine

Role of Extracellular Vesicles in the Association between Air Pollution Exposure and Major Depressive Disorder

Experimental Thesis by

Paola Monti

Supervisor: *Prof. Michele Carugno*

Ph.D. Program Coordinator: *Prof. Carlo Vitantonio Battista La Vecchia*

Academic Year 2023-2024

ABSTRACT

Introduction: Major depressive disorder (MDD) is a common multifactorial condition, with both genetic and environmental causes. Recently, several epidemiological studies have suggested an association between air pollution exposure and MDD; indeed, inhalation of air pollutants such as particulate matter (PM) may promote blood-brain barrier (BBB) disruption and neuroinflammation, possibly exacerbating MDD symptoms. Nevertheless, the biological mechanisms underlying this association remain largely uninvestigated.

Extracellular vesicles (EVs) are a powerful system of intercellular communication that participates in the response to many environmental cues. EVs can cross the BBB and alter its permeability, thus modulating the bi-directional exchange of information between the brain and the periphery. Since EVs can be found in virtually all biological fluids and carry molecular components originating from parental cells, they might provide a non-invasive strategy to study alterations occurring in otherwise inaccessible organs. Of note, alterations in EV profile have been reported under many pathological conditions, including MDD.

Aims of the project: to clarify the biological mechanisms linking air pollution exposure, EVs, and brain pathophysiology. To achieve this aim, the project was divided in two parts: Part 1 was carried out at the EPIGET lab (University of Milan) and aimed at investigating the complex relationship between air pollution exposure, circulating EVs released by neurons (NdEVs), and MDD severity; Part 2 was carried out at the Edinger Institute (Goethe University Frankfurt) and aimed at investigating the effect of EVs released by PM-treated cultured bronchial epithelial cells on an *in vitro* BBB model.

Part 1, materials and methods: 93 patients with MDD were randomly selected from the population of the DeprAir study (a study specifically designed to investigate the association between air pollution and MDD). Daily exposures to air pollutants (NO_2, fine PM) were estimated through a flexible chemical transport model and assigned to study participants according to their residential address. MDD severity was assessed by five different rating scales. The immunoaffinity capture protocol for the isolation of NdEVs was validated by flow cytometry and nanoparticle tracking analysis. The top miRNAs carried by NdEVs were selected by screening 754 miRNAs and analyzed by target prediction/functional annotation. Then, the expression of such miRNAs was quantified

by RT-qPCR in plasma NdEVs from the study population. The collected data were used to evaluate the association between air pollution exposure and the miRNA profile of NdEVs, and between NdEV miRNAs and MDD severity.

Part 2, materials and methods: human bronchial epithelial cells (BEAS-2B) were treated with different concentrations of three types of fine PM (ERM-CZ110, NIST2786, and PM Como), and the effect of such treatment on viability was evaluated by MTT assay and propidium iodide staining. EVs were isolated from the culture supernatant and used to treat a BBB model of mouse brain microvascular endothelial cells (MBMECs). BBB integrity was assessed by measuring trans-endothelial electrical resistance (TEER), as well as by immunocytochemistry.

Part 1, results: The efficacy of the immunocapture protocol of NdEV was higher than 90%. On average, NdEVs accounted for 4.5% of total EVs, and had a smaller size (182 nm vs 218 nm). The top-miRNAs carried by NdEVs were mainly implied in intracellular signaling, cellular responses to stress/external stimuli, immune system regulation, and cell senescence. After performing NdEV miRNA analysis on the 93 study subjects, short-term NO_2 exposure was found to be associated with increased levels of 4 miRNAs (miR-1274B, miR-320, miR-720, miR-451). Instead, miR-19b was positively associated with long-term exposures to both NO_2 and PM with an aerodynamic diameter $\leq$2.5 μm ($PM_{2.5}$). Besides, 10 miRNAs were associated with at least one MDD severity scale. Among them, the brain-enriched, anti-inflammatory miR-451 was found to be negatively associated with MDD severity; similarly, the anti-apoptotic miR-19b was associated with lower MDD severity scores.

Part 2, results: Different PM types were found to elicit different effects on BEAS-2B cell viability, with NIST2786 causing cell death in dose-independent manner. EVs released by BEAS-2B cells treated with 100 μg/ml NIST2786 strongly reduced the TEER of MBMEC monolayers, if compared to EVs released from untreated cells. Such PM-induced EVs also affected the spatial organization of junctional proteins implied in BBB integrity.

Discussion and conclusions: Overall, this study provides novel epidemiological and molecular insights into the role of EVs in mediating the effects of air pollution exposure on the brain. The profiling of NdEV miRNAs could pave the way for the identification of

novel prognostic biomarkers for MDD. Understanding the influence of PM-induced EVs on the BBB might provide new perspectives on the complex mechanisms modulating brain biology in response to peripheral environmental stimuli.

Table of contents

1. INTRODUCTION

1.1. Air Pollution

According to the World Health Organization (WHO), air pollution has been defined as the "contamination of the indoor or outdoor environment by any chemical, physical or biological agents that modifies the natural characteristics of the atmosphere" [1]. Such a broad definition mirrors the great heterogeneity of the substances classified as airborne pollutants, which can originate either from natural sources (e.g. volcanic ash, spores, pollen) or anthropic activities (e.g. agriculture, combustion, or industrial processes) [2]. Based on their physiochemical properties, air pollutants can be divided into two large groups, corresponding to particulate matter (PM) and gaseous molecules.

PM is a mixture of liquid and solid particles that is generally classified according to the aerodynamic diameter (AD) of its components, i.e., the diameter of an equivalent sphere, whose density is 1 /cm^3 (the density of a water droplet), that shows the same behavior in the atmosphere as the irregularly shaped particle. According to this criterion, several classes of PM can be defined. Among the most relevant, we can identify: coarse PM, or $PM_{2.5-10}$, which includes particles ranging from 2.5 to 10 μm; fine PM, or $PM_{2.5}$, which includes particles equal to or smaller than 2.5 μm; and ultrafine PM, or $PM_{0.1}$, including particles equal to or smaller than 100 nm [2]. The AD of the particles determines their capacity to penetrate in the airways: while coarse PM mainly deposits in the nasal cavity and tracheobronchial tree, fine and ultrafine PM can reach the lower respiratory tract, with nanosized particles even making it through the pulmonary alveoli. Here, it could interfere with gas exchanges and even translocate into the bloodstream or nearby tissues, with detrimental effects at both local and systemic levels [2].

On the other hand, the principal outdoor gaseous pollutants include inorganic compounds, like ozone (O_3), carbon monoxide (CO), nitrogen oxides (NO_X, mainly NO_2), and sulfur dioxide (SO_2), as well as volatile organic compounds (VOCs, such as benzene, toluene, and formaldehyde). Due to their low molecular weight and high reactivity, inhaled gaseous pollutants can easily penetrate throughout the human body and cause oxidative stress and cell damage in multiple organs [3,4].

Indeed, nowadays poor air quality represents one of the major environmental threats to human health, with more than 99% of the global population being exposed to concentrations of air pollutants exceeding the WHO safety limits [1]. According to the most recent data provided by the Global Burden of Disease study, PM (either derived from ambient or household air pollution) ranks first among the environmental risk factors generating the greatest global disease burden worldwide, contributing to 8% of total disability-adjusted life-years (DALYs) [5]. Not surprisingly, air pollution exposure has been mainly linked to an increased risk of respiratory and cardiovascular diseases; nevertheless, it is becoming more and more evident that the noxious effects of airborne toxicants are not limited only to directly exposed tissues, thus potentially affecting every organ of the body [6].

1.2. Major Depressive Disorder

Major depressive disorder (MDD) is a disabling mood disorder characterized by a wide spectrum of behavioral and cognitive symptoms, which include persistent low or depressed mood, appetite/sleep disturbances, and loss of interest or pleasure in almost all daily activities [7]. MDD globally affects more than 280 million people (5% of adults) [8] and is foreseen to generate the greatest global burden by 2030 [9,10]. In Italy, the number of people suffering for depression is estimated at 2.8 million [11].

The massive social and healthcare consequences brought about by the high prevalence of this psychiatric disorder are further exacerbated by the limited efficacy of antidepressant treatments, which are successful only in about half of MDD cases [12]; also, there is currently a lack of specific and validated laboratory tests for MDD diagnosis and prognosis, which are therefore based on the symptoms and medical history of the patients [7].

These difficulties are partly due to the fact that this disorder is characterized by a complex pattern of biological alterations, which include unbalanced neurotransmission, hormonal abnormalities linked to hypothalamic–pituitary–adrenal (HPA) axis dysregulation, and impaired neurogenesis and neuroplasticity [13]. More recently, neuroinflammation has been put under the spotlight, as increased levels of pro-inflammatory cytokines have been found in patients with MDD; also, anti-inflammatory drugs have been reported to ameliorate depressive symptoms, while many anti-depressants downregulate inflammation as a side effect [13]. A possible explanation by

which inflammation fosters MDD symptoms revolves around a maladaptive response to infections. Indeed, following an acute infection, anhedonia and fatigue are functional to temporarily give up energy-costing activities such as exploration and mating in favor of healing; however, if inflammation becomes chronic, this "sickness behavior" is no longer adaptive to healing, giving rise to MDD-like pathological outcomes. Besides, the prevalence of MDD is higher in subjects with inflammatory conditions, and patients with MDD have a higher rate of autoimmune diseases if compared to the general population [13].

Although all the discussed mechanisms are likely to be interrelated, every patient might have a distinctive set of pathological alterations, leading in some cases to wrong diagnosis and consequently mistreatment [13].

In addition, such a various set of alterations is thought to be caused by a combination of genetic, biological, environmental, and psychological factors [14,15]. In this regard, recent genome-wide studies have identified more than 200 genes potentially implied in MDD [16]; nevertheless, the limited role played by single genetic polymorphisms has further supported the importance of psychosocial and environmental determinants in the etiology and worsening of MDD [15,17].

1.3. Molecular mechanisms linking air pollution and Major Depressive Disorder

Over the past decades, several epidemiological studies have provided evidence linking air pollution exposure to psychiatric disorders, such as depression [18–20]. The main hypothesis to explain this association is based on the pro-inflammatory and pro-oxidative action of several airborne pollutants, which is exerted through the so-called "direct" and "indirect" pathways (**Figure 1**).

The direct pathway is mediated by gaseous molecules and ultrafine PM, which can first handedly alter the brain physiology via two different mechanisms. On one hand, once inhaled, $PM_{0.1}$ and small gases like NO_2 or CO_2 can enter the bloodstream and reach the BBB, potentially compromising its selective permeability and the capacity to protect the brain from noxious compounds; on the other hand, ultrafine PM might travel by retrograde transportation along the olfactory nerve and reach the olfactory bulb, causing inflammation and neuronal damage [21]. However, experimental evidence supporting a direct action of $PM_{0.1}$ on the brain remains limited and controversial. Instead, the

indirect pathway mediated by bigger particles (such as $PM_{2.5}$ and PM_{10}) is much more consolidated. This route of action consists in the release of many pro-inflammatory mediators (such as cytokines and chemokines) by the airways following to deposition of PM; these signaling molecules can enter the circulatory system and reach the BBB, damaging its selective permeability and consequently leading to loss of brain homeostasis [22].

Figure 1. Effects of air pollution exposure on the brain by direct and indirect pathways. Adapted from Kuntić et al., 2024.

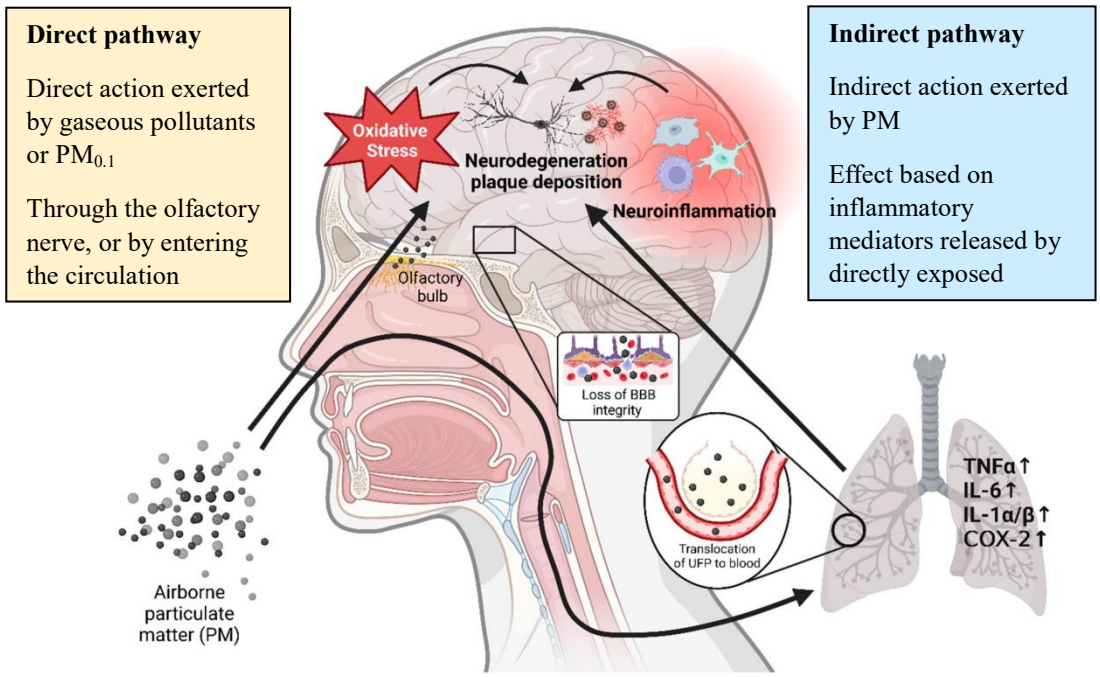

In either the direct or indirect pathway, exposure to air pollutants would result in neurotoxicity and vascular brain lesions, which may trigger or exacerbate the symptoms of depression [23]. Of note, besides the previously described biological alterations, MDD is known to be characterized by impaired BBB functionality [24]; therefore, air pollution might contribute to worsen MDD severity by further compromising BBB properties.

In addition, current knowledge mainly coming from animal models or cell cultures indicates that exposure to environmental stressors can cause epigenetic changes in the brain, including alterations in gene expression regulation mediated by microRNAs (miRNAs), i.e. small non-coding RNA molecules that can interact with target mRNAs

and induce their silencing or degradation [25,26]. Although alterations in miRNA profile have been found in MDD patients if compared to healthy subjects, differences have been mainly observed in post-mortem brain tissue or in peripheral blood [27,28]. Since the expression profile of miRNAs is cell- and tissue-specific, changes in circulating miRNAs might not mirror alterations occurring in the brain. Due to the impossibility of collecting brain biopsies on living patients, the effect of air pollution on brain miRNAs in healthy subjects or in patients with MDD is still completely uninvestigated.

1.4. Extracellular vesicles

Extracellular vesicles (EVs) are lipid bilayer-delimited structures that are generated by almost all cell types and secreted into the extracellular space, where they can enter biological fluids and travel to distant organs [29,30]. Based on their biogenesis, EVs can be classified into two main groups, i.e. exosomes and microvesicles (**Figure 2**).

Figure 2. EV biogenesis and molecular cargo. From Nowak et al, 2023.

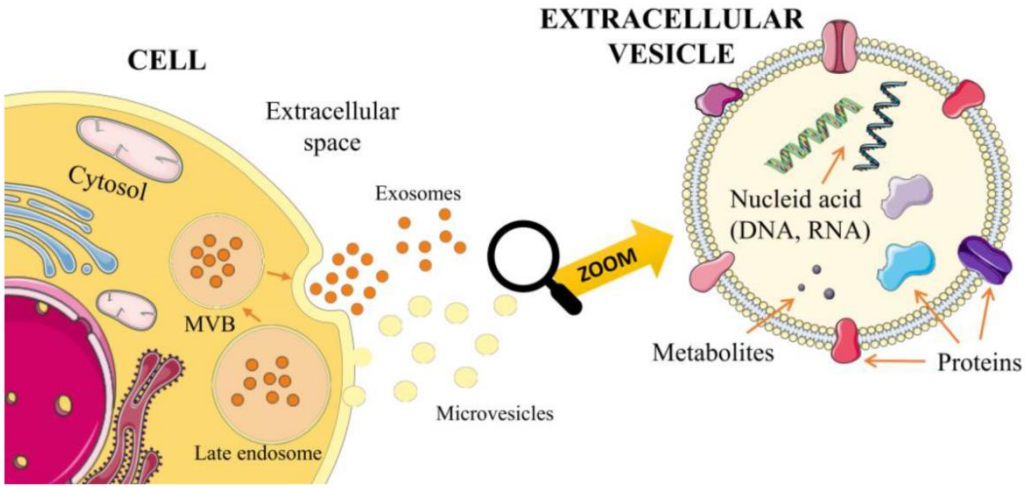

Exosomes, typically ranging between 40-100 nm, are shed in the extracellular space following the fusion of specialized endosomes, called multivesicular bodies (MVBs), with the plasma membrane. MVBs derive from endosomes that underwent intraluminal budding. Instead, microvesicles (generally ranging from 100 to 1000 nm) are directly released outside the cell as they originate from the outward budding of the plasma membrane [31,32].

Originally, little attention has been paid to EVs as they were thought to serve merely as a means to dispose of "cellular garbage" (e.g. misfolded proteins, malfunctioning organelles, etc). However, over time their role has been significantly reconsidered and they are now known to play a key role in exchanging information, either with distant tissues/organs (endocrine signaling) or with nearby cells (paracrine signaling), under both physiological and pathological conditions [33]. Indeed, EVs harbor a variegate cargo of biologically active molecules and organelles, including DNA, RNA (coding and non-coding), proteins, lipids, mitochondria, and various metabolites [29,31]; when encapsulated within EVs, these molecules are protected from degradation [34] and are efficiently internalized [35], with metabolic and epigenetic effects in recipient cells.

Since EVs can been detected in almost all human biological fluids (including blood, urine, saliva, semen, tears, cerebrospinal fluid, and breast milk [36]) and carry a molecular cargo that is representative of the parental cell, they have attracted interest as a minimally invasive source of biomarkers for diagnostic, prognostic and therapeutic purposes [37,38]. Indeed, alterations in the number, size and content of EVs have been observed under many pathological states, either as a consequence of global dysregulation or as part of an adaptive mechanism aimed at restoring homeostasis [39,40]. Of note, the miRNA content of serum EVs has been found to be altered in subjects with MDD [41] and is likely to promote (at least partially) depressive symptoms [42].

1.5. Extracellular vesicles at the interface between the external environment and the brain

Thanks to their pivotal role in cell-cell communication, EVs have emerged as important players in orchestrating the response to external stimuli at a multi-systemic level [43]. In this regard, many environmental stressors (such as air pollution, viral infections, and cigarette smoke) have been reported to enhance the shedding and alter the molecular content of EVs derived from directly exposed tissues; in turn, these environmentally induced EVs could promote adaptation or dysregulation of receiving cells within distant organs, including the brain [43–45]. Indeed, recent studies have shown that EVs released from the periphery of the body are able to cross the BBB and reach the central nervous system [30,46,47].

The BBB is a highly selective, semi-permeable barrier that regulates the bidirectional flow of cells, molecules and ions from the bloodstream to the neural tissue, and *vice versa*, thus maintaining a controlled brain microenvironment and ensuring protection from blood-borne toxic agents [48]. The core anatomical elements of the BBB are endothelial cells of the brain microvasculature, which also interact with pericytes and astrocytes to form a complex functional unit known as neuro-vascular unit [48]. The extracellular spaces between adjacent endothelial cells are sealed by tight and adherens junctions, large supramolecular protein complexes that allow only the passive diffusion of oxygen, carbon dioxide and small lipophilic molecules [48]; instead, all the other compounds can reach the brain only via strictly regulated transport systems. Regarding EVs, the mechanisms of BBB crossing can vary depending on their cellular origin and include adsorptive transcytosis, uptake mediated by specific transporters, or efflux systems [46]. For this reason, EVs have attracted the interest of bioengineers as potential vehicles for the delivery of drugs to the brain, which would have otherwise been excluded from this compartment [49,50].

As in the majority of organs, EVs are thought to play an important role in the functioning of the brain. Here, all the most represented cell subpopulations, including neurons, astrocytes, oligodendrocytes, and microglia, are known to release EVs, which participate in a plethora of physiological processes such as the neuron-glia communication, myelination, waste disposal, and synaptic plasticity [51]. Moreover, brain-derived EVs pose as important regulators of neuroinflammation, promoting disease progression or tissue repair according to their molecular cargo [51]. Of note, also brain-derived EVs can cross the BBB to reach peripheral organs, even though the mode of BBB crossing from this side remains poorly understood [47]; once in the bloodstream, these EVs might be exploited to study alterations occurring in the brain under physiological and pathological states. Indeed, multiple studies have proposed circulating neuron-derived EVs (NdEVs), which are characterized by the presence of the surface protein L1CAM, as a potential source of biomarkers for many neurodegenerative and psychiatric disorders, including Parkinson's disease [52], Alzheimer's disease [53], and autism [54]. Besides, few reports suggest that NdEV cargo might undergo alterations in response to environmental stimuli or lifestyle interventions [55–57]; nevertheless, the impact of air pollution on the content of NdEVs has never been examined before.

2. HYPOTHESES AND AIMS OF THE PROJECT

The general purpose of this project is to investigate the role of EVs in the complex relationship between air pollution exposure and MDD, from both an epidemiological and a molecular perspective.

The first part of the project ("Part 1") was carried out at the EPIGET lab (University of Milan) and aimed at assessing whether exposure to air pollution might influence the miRNA content of neuron-derived EVs (NdEVs), and if changes in such miRNA profile might be associated with MDD severity. MiRNAs are key regulators of gene expression and are known to be responsive to environmental stimuli and pathological states; however, studying miRNA alterations occurring in the brain is highly problematic in living subjects as it would require invasive methods for neural tissue collection. Instead, analyzing the miRNA content of NdEVs, which derive from neurons and therefore carry miRNAs from their parental cell, might be a promising strategy to obtain tissue-specific information regarding epigenetic (dys)regulation occurring in the brain, which might be related to disease severity in patients with MDD.

To verify this hypothesis, I built upon the DeprAir study, a cross-sectional study conducted in the Lombardy region, Italy, whose aim is to understand the interplay between air pollution, different biological variables (blood DNA methylation and plasma levels of inflammatory/hormonal markers), and MDD severity [58]. Here, I introduced an additional biological variable to be tested (i.e., miRNAs from plasmatic NdEVs) to be analyzed on 93 subjects randomly selected from the larger (n=416) DeprAir study population. In detail, the aims of this part of the project are:

1) To characterize the size, number and miRNA content of plasma NdEVs;
2) To predict the gene targets and biological pathways regulated by plasma NdEV miRNAs;
3) To investigate the association between air pollution exposure and NdEV miRNA content in the study population;
4) To investigate the association between NdEV miRNA content and MDD severity in the study population;

5) To try to draw a comprehensive picture of the interplay between air pollution, the miRNA content of NdEVs, and MDD severity in the study population.

The second part of this project ("Part 2") aimed at investigating the EV-mediated effects of PM on the BBB. Here, I hypothesized that fine PM exposure might perturb the homeostasis of directly exposed tissues (i.e., the airways), which in turn might respond by releasing EVs with altered characteristics. Once in the bloodstream, such EVs could participate in the "indirect pathway" as mediators of PM toxicity on the brain by contributing to BBB disruption (which has been observed in many inflammatory diseases, including MDD).

To verify this hypothesis, I pursued a collaboration with Dr. Stefan Momma and Dr. Stefan Liebner at the Edinger Institute (Goethe University, Frankfurt). Here, I established a protocol to treat the human bronchial epithelial BEAS-2B cells (chosen as a paradigm of directly exposed cells) with PM; as the biochemical composition of PM can vary a lot depending on its origin, three different types of fine PM (derived from urban areas, road tunnels or indoor environments) were tested. After treatment, EVs released by BEAS-2B cells were used to treat mouse brain microvascular endothelial cells (MBMECs), taken as an *in vitro* BBB model. In detail, the aims of this part of the project are:

1) To investigate the effect of treatment with three different PM types on BEAS-2B cells;
2) To investigate the effect of EVs released by PM-treated BEAS-2B cells (versus non-treated) on the functional properties of MBMECs (trans-endothelial electrical resistance);
3) To investigate the effect of EVs released by PM-treated BEAS-2B cells (versus non-treated) on the biochemical properties of MBMECs (spatial organization of junctional proteins).

3. MATERIALS AND METHODS

3.1. PART 1

As summarized in **Figure 3**, 93 subjects with MDD were randomly sampled from the DeprAir study population. For each subject, after signing of informed consent, socio-demographic and lifestyle data were collected by questionnaires, and MDD severity was evaluated by trained physicians. Air pollution exposure was estimated using a chemical transport (FARM) model. Besides, each participant donated a blood sample, which was used to isolate plasmatic neuron-derived EVs (NdEVs) by immunoaffinity capture. After characterizing plasma NdEVs and selecting miRNA candidates, target prediction analysis and functional annotation were performed on the top-miRNAs identified within EVs. Then, the expression levels of the selected NdEV miRNAs were evaluated by qPCR (OpenArray technology) on the study population. Associations between air pollution exposure, miRNAs, and MDD severity were assessed by appropriate statistical models (see below).

Figure 3. Workflow of Part 1.

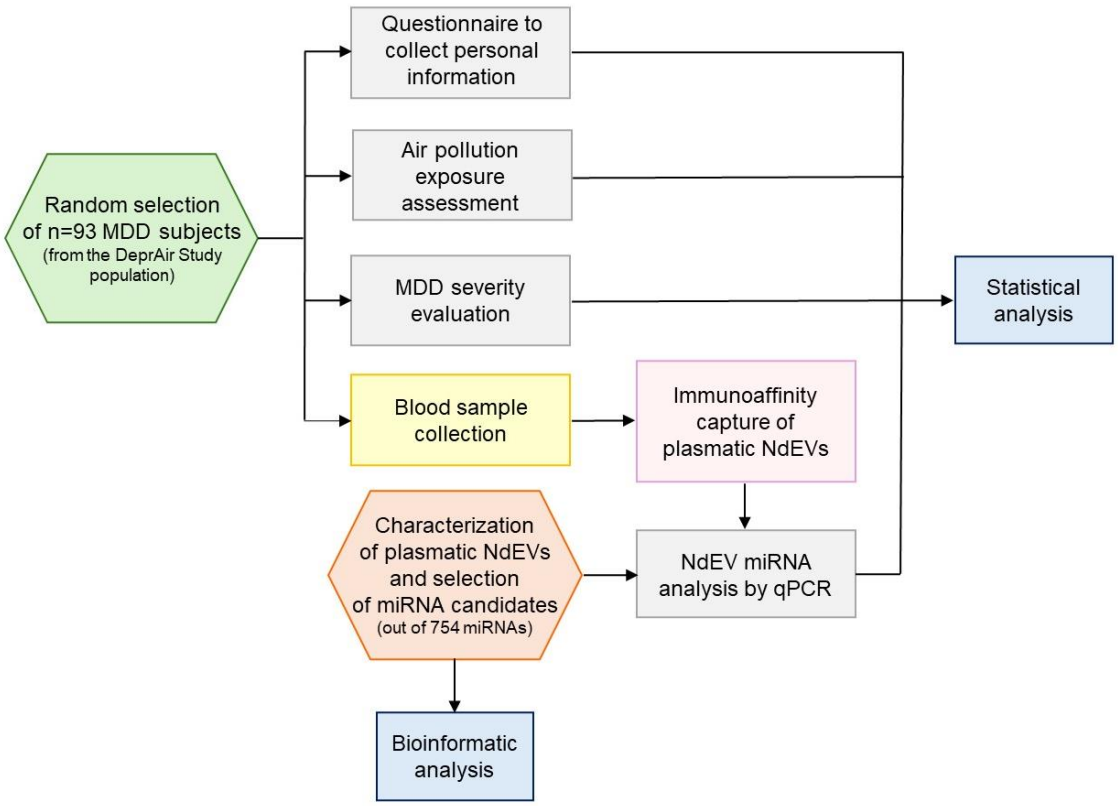

3.1.1. Subject recruitment and characteristics

This study involves 93 patients with MDD. These patients were randomly sampled from a larger population (n=416) recruited between September 2020 and December 2022 in the context of the DeprAir study (CARIPLO Foundation - 2019-3354; https://deprair.com/en/homepage/) [58]. All study participants were enrolled at the Psychiatry Unit of the Fondazione IRCCS Ca' Granda Ospedale Maggiore Policlinico (Milan), either as incident cases or as outpatients, who have been accessing the hospital since 2003 for MDD. Subjects of both sexes aged 18-65 and with a previous diagnosis of MDD were considered eligible for this study. Exclusions criteria were the following: having medical conditions potentially associated with behavioral disorders (e.g., hypothyroidism, previous stroke), drug abuse in the previous month, other psychiatric disorders (except for personality disorders other than borderline disorder), medical conditions or treatments that are likely to alter inflammatory parameters (e.g., autoimmune diseases, steroids or interferon treatment), infectious diseases, pregnancy.

By signing a detailed informed consent form, all participants agreed to: provide access to personal information from medical records, donate a 30 ml blood sample, and fill in two questionnaires to collect sociodemographic data, recent residential history, lifestyle (i.e., smoking habits, diet), clinical history for selected diseases (hypertension, hypercholesterolemia, diabetes, cancer, heart disease, renal failure), and clinical history for depression.

3.1.2. Assessment of MDD severity

MDD diagnosis was confirmed using the Structural Clinical Interview for DSM-5 (SCID - Italian version). Depression severity was assessed with the following rating scales:

- Montgomery-Asberg Depression Rating Scale (MADRS): this scale evaluates core symptoms of MDD. It comprises 10 items: apparent sadness, reported sadness, inner tension, reduced sleep, reduced appetite, concentration difficulties, lassitude, inability to feel, pessimistic thoughts, suicidal thoughts. Each item is rated from 0 to 6, with higher scores reflecting more severe symptoms. Ratings can be summarized in an overall score (from 0 to 60), which

allows to stratify severity of depression as: 0–6: no depression, 7–19: mild depression, 20–34: moderate depression, ≥35: severe depression [59];

- Hamilton Depression Rating Scale (HAM-D) 21-item: this scale evaluates anxiety and somatization symptoms of MDD. It comprises 21 questions on depression-related symptoms (e.g. anxiety, mood, insomnia) and somatic symptoms experienced within the past week. Each symptom is rated on a scale of 0-2, 0-3, or 0-4 (the highest the score, the most severe the symptoms). Based on the overall score (from 0 to 67), which is obtained by summing single ratings, severity of depression can be stratified as: 0–7: no depression, 8–16: mild depression, 17–23: moderate depression, ≥24: severe depression [60];
- Clinical Global Impression-severity of illness (CGI): this scale evaluates the global severity of illness based on the psychiatrist's answer to the following question: "Considering your total clinical experience with this particular population, how mentally ill is the patient at this moment?". The answer can range from 1 to 7, where: 1= normal, not at all ill; 2= borderline mentally ill; 3= mildly ill; 4= moderately ill; 5= markedly ill; 6= severely ill; 7= among the most extremely ill patients [61];
- Sheehan Disability Scale (SDS): this scale evaluates the social dysfunction associated with MDD. It consists of a self-reported assessment of functional impairment composed of five items. The first three are global rating scales which assess impairment in work, home, and family responsibilities. There are two additional questions which measure perceived stress and social support. The items are scored individually on 10-point numerical rating scales, except for the "social support" one that can be scored 0-100 [62];
- Global Assessment of Functioning (GAF): this scale evaluates the overall impairment associated with MDD, by measuring how much a person's symptoms affect his/her day-to-day life on a scale from 0 to 100. The higher the score is, the better the patient can cope with daily activities, suggesting that a lower score indicates a greater social dysfunction associated with depression [63].

3.1.3. Assessment of air pollution exposure

Air pollution exposure was assessed for particulate matter with AD less than or equal to 2.5 μm ($PM_{2.5}$), and nitrogen dioxide (NO_2). First, each patient's residential address was translated into spatial coordinates using the web tool GPS Visualizer (https://www.gpsvisualizer.com) and geocoded using QGIS (http://qgis.osgeo.org). Then, air pollution exposure levels were assigned to each study participant using daily mean estimates derived from the Flexible Air quality Regional (FARM) model of the Lombardy region environmental protection agency (ARPA Lombardia), which are available as daily means at a 1x1 km resolution or at municipality level [64]. Daily estimates of each pollutant's exposure were obtained for each day starting from the day of recruitment (day 0) to 365 days before recruitment (day 365).

Daily estimates of the day of recruitment (day 0) and the preceding one (day -1) were used as representative of short-term exposure to air pollution. On the other hand, to analyze long-term effects of air pollution, two different time windows were calculated (i.e., moving averages) by averaging pollutant levels of the day of recruitment with the levels of each preceding day up to 180 days (lag 0-180), and 365 days before (lag 0-365).

Exposure to apparent temperature (AT), which is a measure of temperature that considers also humidity and wind speed, was also estimated. Daily means of temperature, humidity, and wind speed were retrieved from the weather monitoring stations of ARPA Lombardia and then assigned to each subject considering the closest station to his/her residential address. AT was estimated following the formula that can be found in [65]. The same multiple time windows of exposure to air pollutants were estimated and considered in the analyses.

3.1.4. Collection of blood samples and EV isolation

Blood drawing was performed directly by the recruiting physician. 30 ml blood samples were collected into five EDTA tubes, which were centrifuged at 1200 g for 15 min at room temperature (RT) to separate plasma and buffy coat fractions [66]. In order to preserve the physiochemical characteristics of plasmatic EVs, plasma samples were stored at -80°C with the addition of 0.04 M sucrose and thawed only once. To isolate EVs, 1.6 mL plasma was added with 0.1 μm-filtered Phosphate Buffered Saline (PBS)

to a final volume of 5 mL, and the tube was centrifuged at 1000, 2000 and 3000 g for 15 min at 4°C. The resulting pellet of cell debris was discarded, while the supernatant was ultracentrifuged at 110,000 g for 75 min at 4 °C to obtain an EV-rich pellet.

3.1.5. Immunoaffinity enrichment of neuronal EVs

The enrichment of neuron-derived EVs (NdEVs) was carried out by immunoaffinity capture, according to the protocol described in [67], with minor modifications. After adding bovine serum albumin (BSA, #A7030, Sigma) and protease and phosphatase inhibitors (PPI, #78447, LifeTechnologies) to the EV-rich pellet resuspended in 0.1 µm triple-filtered PBS, total EVs were incubated with an anti-L1CAM biotinylated antibody (1:150, eBio5G3, #13-1719-82, Invitrogen) for 1 hour on a rotating wheel. Following addition of pre-washed Pierce Streptavidin Plus UltraLink Resin (#53116, LifeTechnologies) for 30 min on a rotating wheel, the suspension was centrifuged at 200 g for 10 min to obtain an EV pellet enriched with L1CAM+ EVs. Then, after removing the supernatant, each sample was added with Buffer Gly-HCl pH 3.0 0,1M (#24074, Polysciences) and incubated for 10 min on a rotating wheel, thus causing the dissociation of L1CAM+ EVs from the beads. Samples were then centrifuged at 4500 g for 10 min to pellet the beads, and the supernatant containing L1CAM+ EVs was collected and added with PPI and Buffer Tris HCl pH 8.0 1M (#J22638.AE, LifeTechnologies) to neutralize the acidic buffer. Samples were finally stored at -20°C.

3.1.6. Flow cytometry and Nanoparticle tracking analysis

Flow cytometry analysis was carried out using the MACSQuant® Analyzer (Miltenyi Biotec) according to the protocol reported in [68]. To evaluate EV integrity, sample aliquots were stained with 200 nM 5(6)-carboxyfluorescein diacetate N-succinimidyl ester (CFSE) at 37 °C for 30 min in the dark. After CFSE staining, EVs were incubated with anti-L1CAM primary antibody (1:100, EPR18750, #ab208155, Abcam) for 30 min at 4°C, followed by incubation with Alexa Fluor 647- conjugated secondary antibody (1:100, #A21245, Invitrogen) for 30 min at 4°C in the dark. Data analysis was conducted using FlowJo (v. 10.8.1, Becton Dickinson).

The concentration (count/ml) and size distribution (0-1000 nm) of EVs were assessed by Nanoparticle Tracking Analysis (NTA), a technique that measures the Brownian motion of particles suspended in fluid, as described before [69]. Using the NanoSight

NS300 system (Malvern Panalytical Ltd., Malvern, UK), EVs were detected by laser light scattering and displayed in real time through a high sensitivity Charge-Coupled Device (CCD) camera. Four total EV samples (derived from plasma pools of healthy subjects) and four NdEVs samples (isolated from an aliquot of total EV samples) were employed for this analysis. Five 30s recordings were made for each sample. Collected data were analyzed with the NTA software (v. 3.3, Malvern Instruments Ltd).

3.1.7. Extraction of EV miRNAs

EV miRNAs were extracted using the miRNeasy mini Kit and RNeasy MinElute Cleanup Kit (#217004 and #74204, Qiagen). Briefly, 200 µl of NdEV samples were added with 1 ml QIAzol Lysis Reagent, mixed thoroughly, and incubated for 5 min; then, samples were added with 200 µl of chloroform and shaken vigorously for 30s. After incubation for 3 min, samples were centrifuged for 15 min at 12000g 8°C, and the aqueous phase was mixed with an equal volume of Ethanol 70%. The resulting solution was subsequently loaded onto an RNeasy Mini spin column and centrifuged for 30s at 11000g 20°C to remove long RNA molecules. The eluate was then added with 830 µl of Ethanol 100%, mixed thoroughly, transferred onto a RNeasy MinElute spin column, and centrifuged for 30s at 11000g 20°C. The column was then washed with 500 µl of RPE Buffer and centrifuged for 30s at 11000g 20°C, followed by washing with 500 µl of Ethanol 80% and centrifuging for 2 min at 11000g 20°C. After repeating the centrifugation with empty column for 5 min at 11000g 20°C to dry the membrane, 20 µl of RNAse-free water was added on top of the filter and incubated for 5 min. miRNAs were eluted by centrifuging for 1 min at 11000g 20°C and stored at -80°C. The quality of the extracted miRNAs was determined using the 2100 Bioanalyzer (Agilent).

3.1.8. Preliminary screening of neuronal EV miRNAs

Next, miRNAs were subjected to reverse transcription and pre-amplification, followed by real-time PCR with the QuantStudio™ 12 K Flex OpenArray® Platform (QS12KFlex, Applied Biosystems), as described in [66].

First, a preliminary screening of NdEV miRNA content was carried out by profiling 754 unique miRNAs on 3 pools of plasma samples from healthy donors and 3 pools from subjects with MDD. For each pool, total EVs and NdEVs were analyzed.

After concentrating extracted miRNAs with the Concentrator plus (Eppendorf), reverse transcription was performed using the TaqMan® Micro RNA Reverse Transcriptase Kit (Life Technologies) with the Megaplex™ RT Primers, Pool A v2.1 and Pool B v3.0. Two distinct reactions were performed to cover all 754 target miRNAs (plus 16 replicates of four internal controls: ath-miR159a, RNU44, RNU48, and rRNA U6). Each reaction included: 0.75 µl of Megaplex RT Primers Pool A or Pool B, 0.15 µl of deoxynucleoside triphosphates (dNTPs,100 mM), 0.75 µl of 10X RT Buffer, 0.90 µl of $MgCl_2$ (25 mM), 0.1 µl of RNase Inhibitor (20 U/µl), 1.5 µl of MultiScribe™ Reverse Transcriptase (50 U/µl), and 3.3 µl of miRNAs. After incubation on ice for 5 min, the mixture was subjected to the following thermal protocol in a C1000 Thermal Cycler (Biorad): 40 cycles of 16 °C for 2 min, 42 °C for 1 min, and 50 °C for 1 s, plus one cycle at 85 °C for 5 min. The copy DNA (cDNA) samples were stored at -20 °C until use. Then, cDNA was loaded onto a 96-well plate for pre-amplification. Briefly, 7.5 µl of each reverse-transcribed miRNA was combined with the following reaction mix: 20 µl of TaqMan® PreAmp Master Mix (2X), 8.5 µl of nuclease-free water, and 4 µl of Megaplex™ PreAmp Primers Pool A or B (10X). Thermal conditions for the pre-amplification reaction were as follows: 95 °C for 10 min, 55 °C for 2 min, 72 °C for 2 min, 16 cycles of 95 °C for 15 s and 60 °C for 4 min, and 99.9 °C for 10 min. Pre-amplified cDNA was then diluted 1:20 with nuclease-free water, and added with TaqMan Open Array® Real Time PCR Master Mix (2X) in a 1:1 volume ratio. Finally, 7 µl of the reaction mix was aliquoted with the MicroLab STAR Let instrument (Hamilton Robotics) into eight wells of a 384-well OpenArray® plate. The reaction mix was then loaded from the 384-well plate into a TaqMan™ OpenArray® Human miRNA Panel, using the QuantStudio™ AccuFill System Robot (Life Technologies). The mixture was analyzed with the QuantStudio™ 12K Flex Real-Time PCR System (software v.1.2.2) with the OpenArray® Platform (QS12KFlex), according to the manufacturer's instructions.

Gene Expression Suite Software (Life Technologies) was used to process miRNA expression data from the miRNA panel. MiRNAs with a Ct<28 and AmpScore>1.20, which were present in >1/6 NdEV samples, were selected for miRNA analysis on the study population. Regarding miRNAs that were present only in 1/6 NdEV samples, they were considered only if they were found in a MDD pool (i.e., miRNAs identified only

in one pool of healthy subjects were excluded). The NormFinder algorithm was used to choose the best normalization strategy [70]. Expression levels were calculated as $RQ=2^{-\Delta Ct}$, where ΔCt= Ct(measured) – Ct(normalization).

3.1.9. Analysis of neuronal EV miRNAs in the study population

The selected miRNAs and internal controls were then quantified in triplicate in the study population using Custom miRNA OpenArray® Plates, following a similar procedure to the one described in the previous paragraph (also described in [66]). Briefly, reverse transcription was carried out using the Custom Primers Pool and TaqMan® Micro RNA Reverse Transcriptase Kit (Life Technologies). Each reaction included: 3 µl of RT Primers Pool, 0.15 µl of dNTPs (100 mM), 0.75 µl 10X RT Buffer, 0.09 µl of RNases Inhibitor (20 U/µl), 1.5 µl of MultiScribe™ Reverse Transcriptase (50 U/µl), and 2.01 µl of miRNAs. Then, the mixture was subjected to the following thermal protocol in a C1000 Thermal Cycler (Biorad): 16 °C for 30 min, 42 °C for 30 min, and 85 °C for 5 min. The cDNA samples were stored at -20 °C until further use.

Each cDNA was then pre-amplified in a 96-well plate, in a reaction mix that included: 12.5 µl of TaqMan® PreAmp Master Mix (2X), 10 µl of nuclease-free water, 10 µl of PreAmp Custom Primers Pool (4X), and 7.5 µl of reverse-transcribed miRNA. The thermal profile of pre-amplification, as well as the procedures for sample dilution, loading, and analysis, were the same as in the screening phase, with the exception that 6 µl of reaction mix was aliquoted with the MicroLab STAR Let robot (Hamilton Robotics, Birmingham, UK) into three wells of a 384-well OpenArray® plate. Also, only miRNAs with a Ct<28 and AmpScore>1.24, and that were detected in >70% samples, were considered for statistical analysis. NormFinder was used to select the best normalization strategy among U6-snRNA, ath-miR159a and the mean of these two miRNAs [70]. The latter was selected as the best normalization method. MiRNA expression was determined using the relative quantification $2^{-\Delta Crt}$.

3.1.10. Bioinformatic and statistical analyses

The miRNA Enrichment Analysis and Annotation tool (miEEA) was utilized to perform functional enrichment and over-representation analysis (ORA) on the selected 52 miRNAs [71]. Selected miRNAs were primarily mapped to their validated target genes using miRTarBase [72]. Reactome was chosen within miEEA for the enrichment analysis,

facilitating accurate mapping of miRNA target genes to biological pathways [73]. miEEA performed ORA by conducting hypergeometric tests to evaluate the significance of the overlap between the miRNA target genes and the genes associated with each pathway in Reactome. The null hypothesis assumed that any observed overlap was due to random chance. To ensure robustness and biological relevance, only pathways with a p-value < 0.01 and involving at least 10 miRNA target gene hits were considered significant. Due to the high number of comparisons, a multiple comparison correction method based on the Benjamini-Hochberg False Discovery Rate (FDR) was applied to all the analyses to calculate the FDR p-value.

Descriptive analyses of study population characteristics, variables describing characteristics of MDD, and related severity scales were performed. Principal exposure windows of $PM_{2.5}$ and NO_2 used in the analyses were also summarized. Continuous variables were summarized as means with corresponding standard deviations, after having checked for normality. Categorical data were synthetized reporting absolute and relative frequencies.

To study the association between different air pollutants exposure and miRNA expression, multivariate linear regression models were used, after applying a log2-transformation of miRNA expression to achieve normal distribution. Models were adjusted for AT (same lag as for air pollution), gender, age, occupation, education, month and year of recruitment, antidepressant treatment (yes vs. no), body mass index (BMI), smoking and OpenArray plate. Results were expressed as regression coefficients or slopes (β) per 10 $\mu g/m^3$ increase in air pollutants concentrations, with corresponding 95% confidence intervals (95% CI).

Multivariate linear regression models were also used to evaluate the association between miRNA expression and MDD severity for all the scales, except for CGI where a multivariate ordinal regression model was used, due to the ordinal nature of this scale. Models were adjusted by gender, age, occupation, education, month and year of recruitment, antidepressant treatment (yes vs. no), BMI, smoking and OpenArray plate. Also in these models, miRNA expression data were log-transformed.

The Benjamini-Hochberg procedure was applied to adjust for multiple comparisons and calculate the FDR p-value. Analyses were performed using Stata (Stata Corp. 2023; Stata Statistical Software: Release 17; College Station, Texas, USA: Stata Corp LLC).

3.2. PART 2

As schematized in **Figure 4**, human bronchial epithelial cells (BEAS-2B) were treated with PM, and reduction of cell viability was measured by [3-(4,5-Dimethylthiazol-2-yl)-2,5-Diphenyltetrazolium Bromide] (MTT) assay and propidium iodide staining. Then, EVs released after PM treatment (vs. control) were collected. BEAS-2B EVs were used to treat primary endothelial cells (MBMECs) isolated from mouse brains. After seeding the cultured cells onto transwell inserts, the effect of such treatment was evaluated by different assays (i.e., trans-endothelial electrical resistance - TEER measurement and immunocytochemistry) to assess functional and molecular alterations in BBB properties.

Figure 4. Workflow of Part 2.

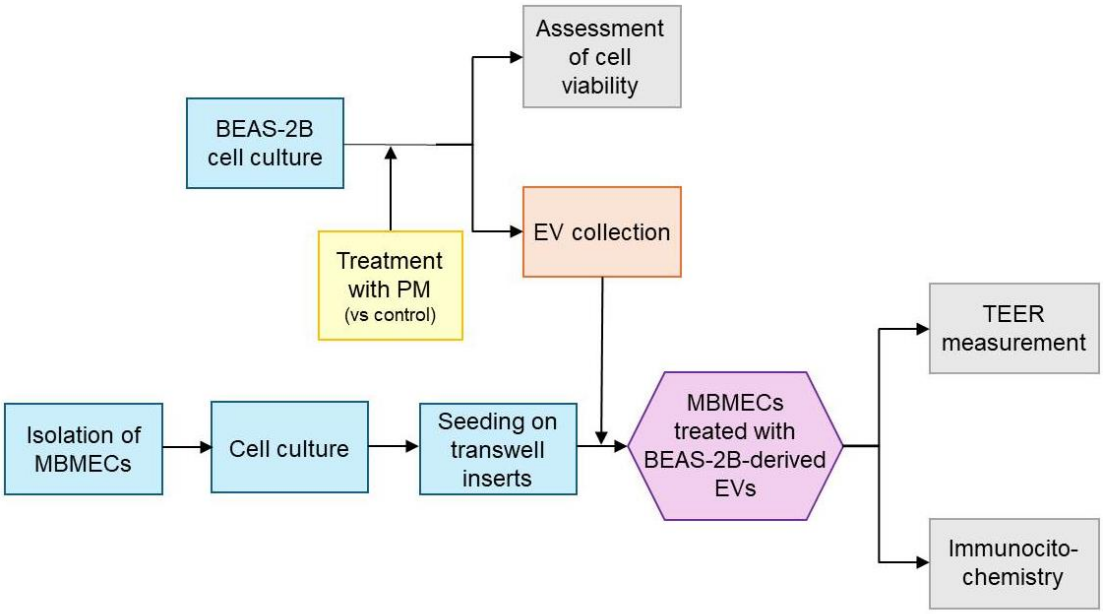

3.2.1. Particulate matter

Three PM types were employed for the experimental analyses (**Table 1**). Fine dust, $PM_{2.5}$-like reference material (ERM-CZ110, [74]) and fine particulate matter <4 μm standard reference material (NIST2786, [75]) were purchased by Sigma-Aldrich. In addition, urban $PM_{2.5}$ collected in Como (Lombardy, Italy) using high-volume air samplers, as described in [76], was kindly provided by Prof. Andrea Cattaneo (University of Insubria, Como, Italy).

Table 1. Characteristics of the three PM types. For NIST2786, data concerning polycyclic aromatic hydrocarbons, brominated diphenyl ether congeners, hexabromocyclododecane isomers, sugars, polychlorinated dibenzo-p-dioxin and dibenzofuran congeners have been omitted for brevity.

	PM type		
	ERM-CZ110	NIST2786	Como PM
Origin	Road tunnel in Warsaw (Poland)	Exhibition center in Prague (Czech Republic)	Urban outdoor site in Como (Italy)
Year of collection	2006	2005	2019
Reference material	Yes	Yes	No
AD (nm)	<2.5	<4	<2.5
Chemical composition			
Ionic components (mg/g)			
NO_3^-	7.8	NA	218
SO_4^{2-}	75	NA	108
Cl-	26.2	NA	13.9
Na^+	20.4	NA	44.2
NH_4^+	1.3	NA	47.4
K^+	3.3	NA	28.1
Mg^{2+}	1.8	NA	20.3
Ca^{2+}	44	NA	34.0
Elements (μg/g)			
Na	23000	14920	NA
K	8500	NA	NA
Ca	65000	73500	NA

Mg	9200	8300	NA
Fe	NA	48900	1844
Zn	NA	1793	1882
Mn	NA	780	180
Cu	NA	847	147
Sr	NA	NA	72.4
Pb	NA	286	66.8
Cr	NA	462.2	41.5
Ni	NA	243	33.3
Hg	NA	5.32	NA
Al	NA	33480	NA
Sb	NA	192.1	NA
Cs	NA	4.01	NA
Cl	NA	17390	NA
La	NA	20.72	NA
Sm	NA	2.840	NA
Ti	NA	2460	NA
V	NA	85.5	26.4
As	NA	36.7	6.8
Se	NA	NA	5.0
Co	NA	19.55	1.8
Cd	NA	4.34	0.9
Carbonaceous fractions (mg/g)			
Organic carbon	NA	NA	141
Organic matter	NA	NA	225
Elemental carbon	NA	NA	5.3

3.2.2. Cell cultures and growth conditions

Human bronchial epithelial cells BEAS-2B were kindly provided by Prof. Cristiana Stellato (University of Salerno, Italy) and cultured in Dulbecco's Modified Eagle Medium (DMEM)/ F-12 (1:1) 1X + GlutaMAX^{TM} (31331-028, Gibco), supplemented with 5% fetal bovine serum (FBS, #P30-3702, Pan Biotech), 2 mM L-Glutamine solution (#G7513, Merck), and 2 mM penicillin/streptomycin solution (P/S, #P4333, Merck).

Primary mouse brain microvascular endothelial cells (MBMECs) were cultured in MCDB-131 (10372-019, Gibco), 20% FBS (#F7524, Merck), 2 mM L- Glutamine solution, 2 mM P/S solution, 50 ng/ml endothelial cell growth supplement (ECGS, homemade, from pig brain; alternatively, #E2759 Sigma-Aldrich), 0.1 mg/ml heparin (#H4784 Sigma-Aldrich), and 1 mg/ml sodium bicarbonate.

All cell lines were grown at 37°C and 5% CO_2. Cells were routinely split with Trypsin 0.05 %/EDTA and stored in liquid nitrogen in DMSO 10% FBS.

3.2.3. Preparation of MBMECs

MBMECs were freshly isolated from brains of C57BL/6J mice, as previously described in [77]. Briefly, after carefully removing the meninges and the choroid plexus, brains were washed in Buffer A (For a 500 ml solution: 4,47 g NaCl; 0,2087 g KCl; 0,1276 g CaCl2; 0,1237 g MgCl2; 1,78725 g HEPES; 5 g BSA Grade V; H2O mq to volume) filtrated with 0,22 µm pore size, and homogenized. After centrifuging the homogenate at 1500 rpm, 4°C for 10 min, the resulting pellet was resuspended in equal volumes of Buffer A and 0,75% Collagenase A (#10103578001, Merck) in Buffer A, added with 4 µg/ml DNAse (#LS006331, Worthington). This first digestion step was carried out for 60 min at 37°C under shaking (600 rpm).

After stopping collagenase digestion by adding excess Buffer A, samples were centrifuged for 10 min at 1500 rpm 4°C, and the pellet was carefully resuspended in PBS with BSA 25% (double-filtered with 5,0 µm and 0,45 µm pore size filters); by centrifuging for 20 min at 3000 rpm 4°C, the BSA gradient allows the separation of myelin and BSA from the cell pellet, which is subsequently resuspended in Buffer A added with 1% Collagenase/Dispase solution (#10269638001, Roche) and 4 µg/ml DNAse I. This second digestion step was carried out for 30 min at 37°C under shaking (600 rpm) and stopped by adding excess Buffer A. After centrifuging for 5 min at 1500 rpm 4°C, the cell pellet was washed with Buffer A and centrifuged again for 5 min at 1500 rpm 4°C. The pellet was then resuspended in culture medium and cells were seeded on a 6-well dish previously coated with Collagen Type I (#354236, Corning). Endothelial cells were selected by treatment with 4µg/ml puromycin dihydrochloride (#P9620, Sigma).

3.2.4. MTT assay

BEAS-2B cells were seeded at a concentration of 2×10^4 cells/well in a 96-well plate, and treated the following day with different concentrations of pollutants (200, 100, 50, 25, 12,5, and 0 μg/mL, in triplicate) for 24 hours. Three wells were treated with a 10% ethanol solution, as a positive control of cell death. Then, the percentage of viable cells was determined by MTT assay using the Cell proliferation kit I (#11465007001, Roche), according to the manufacturer's instructions. Following the 24 hour-treatment, cells were washed once with PBS, and each well was added with 100 μL fresh medium and 10 μL MTT labeling reagent. After 4 hours of incubation at 37°C, each well was added with 100 μL pre-warmed solubilization buffer. The following day, absorbance was measured at λ=565 nm using the Infinite 200 PRO plate reader (Tecan).

3.2.5. Propidium iodide staining and flow cytometry

After seeding 2×10^4 BEAS-2B cells in a 96-well plate and treating them with different PM types and concentrations, as described in the previous section, cells were also stained with propidium iodide (PI, #P4864, Sigma-Aldrich) and analyzed by flow cytometry. Treatment with 10% ethanol was performed as a positive control. After the 24-hour PM treatment, cells were incubated with PI 1μg/ml for 10 minutes at 37°C; then, cells were washed with PBS and detached with tripsin. Cells were then collected and centrifuged at 600 rpm for 4 minutes; after removing the supernatant, cells were resuspended in PBS with 1% serum and PI staining was assessed using the BD FACSCanto II flow cytometer (BD Biosciences). Data were visualized and analyzed using the BD FACSDiva software (v. 6.1.3, BD Biosciences).

3.2.6. Cell treatments and EV collection

After seeding 10^6 BEAS-2B cells on 10 cm^2 petri dishes in quadruplicate per condition, the following day the growth medium was substituted with a fresh one containing 5% EV-depleted serum, which was obtained by ultracentrifuging serum at 30000 rpm for 22 hours (Sorvall WX Ultra series ultracentrifuge, Surespin 630 rotor).

Cell treatments with PM and EV collection were carried out as schematized in **Figure 5**. EVs were collected from: 1) untreated BEAS-2B cells, 24 h after adding medium with EV-depleted serum; 2) treated BEAS-2B, i.e. cells treated with 100 μg/ml NIST2786 in

medium with EV-depleted serum, for 2h or 24 h; 3) "post-treated" BEAS-2B, i.e. BEAS-2B cells that have been treated for 24h with 100 µg/ml NIST2786, washed carefully with PBS for 3 times (to remove residual traces of PM), and then incubated again for 2h with fresh medium with EV-depleted serum.

Figure 5. Cell treatments and EV collection workflow.

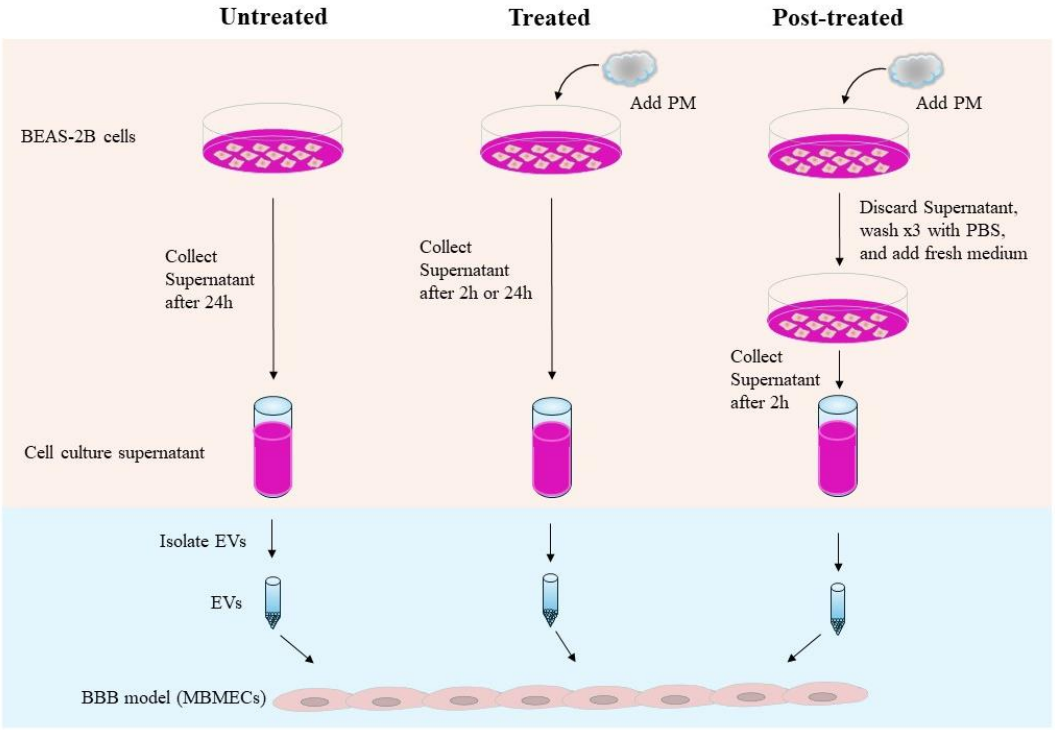

Concerning the treated and post-treated conditions, PM was resuspended in an appropriate volume of culture medium; then, the PM suspension was sonicated at 45 Hz for 10 min with the Bransonic 32 Ultrasonic cleaner, sterilized under UV light for at least 1 hour, and carefully resuspended by pipetting and vortexing before starting the cell treatment. For EV isolation, cell culture supernatants were collected after 24 hours from treatment. Instead, to obtain post-treatment EVs, PM-treated cells were thoroughly washed 3 times with PBS and were incubated with fresh medium, which was collected after 2 hours. The cell supernatants were then centrifuged at 300g, 4°C for 10 min; after discarding the pellet, the resulting supernatant was centrifuged again at 1000g, 4°C for 20 min. Then, the supernatant was added with 10% Polyethylene glycol 6000 (PEG, #A1387, PanReac AppliChem) and incubated overnight at 4°C. The next day, samples were centrifuged at 3000g, 4°C for 45 min; after discarding the supernatant, the pellet

was resuspended in 10 mM HEPES buffer pH 7.5 (#A6916, PanReac AppliChem) and ultracentrifuged (Sorvall WX Ultra series ultracentrifuge, FIBERLite F45L-24×1.5 rotor) at 31000 rpm, 4°C for 2 hours. The EV-rich pellet was then resuspended in 10 mM Hepes buffer pH 7.5 and stored at 4°C until use.

3.2.7. TEER measurement

Trans-endothelial electrical resistance (TEER) was conducted using the cellZscope system (nanoAnalytics, Münster, Germany), as described in [78]. First, transparent polyethylene terephthalate ThinCert™ transwell inserts with 1.0 µm pore size (#662610; Greiner Bio One) were coated with 1% collagen type 1 and 1% fibronectin in PBS for at least 1 hour at 37°C. Then, MBMECs were briefly washed twice in PBS and detached with tripsin. After neutralizing tripsin with MBMEC complete medium, cells were centrifuged at 1000g for 3 min, and resuspended in MCDB-131 basal medium to remove serum. Then, cells were centrifuged again at 1000g for 3 min, resuspended in MBMEC medium with 20% EV-depleted FBS, and counted. After washing the inserts twice with PBS, approximately 5×10^5 cells in 320 µl EV-depleted MBMEC medium were seeded on top of each insert, and incubated at 37°C for at least 1 hour in order to attach to the porous membrane. Finally, each insert was transferred into the cellZscope device (NanoAnalytics), whose wells were previously filled up with 1 ml EV-depleted MBMEC medium. The cellZscope system was then placed in a dedicated cell incubator, and TEER measurements were automatically registered every 10 minutes for at least 5 days using the dedicated cellZscope software (v. 1.5.3, NanoAnalytics). In parallel, the same apparatus also monitored cell capacitance (C_{cl}).

3.2.8. Immunofluorescence

Immunofluorescence was performed on transwell inserts at the measurement endpoint. After fixing the cells with cold methanol for 3 min, the porous membranes were washed with PBS and cut off from the transwell inserts. Then, membranes were incubated for 1 h with a permeabilization/blocking solution, i.e. PBS supplemented with 10% normal donkey serum (#D9663, Merck) and 0,1% Triton X-100, followed by incubation overnight at 4°C with primary antibody solution (PBS supplemented with 1% normal donkey serum and 0,1% Triton-X, added with appropriate dilutions of primary antibodies). The tested primary antibodies were: anti-claudin 5 (1:200, #34-1600,

Invitrogen), and anti-VE-cadherin (1:100, #00105rs, BiCell Scientific). The following day, cells were washed 3 times with PBS and incubated with secondary antibody solution (PBS supplemented with 1% normal donkey serum and 0,1% Triton-X, added with appropriate dilutions of secondary antibodies). The following secondary antibodies were used: Donkey anti-Rabbit IgG (H+L) Cross-Adsorbed Secondary Antibody, DyLight™ 650 (1:1000, #SA5-10041, Invitrogen), and Donkey anti-Rat IgG (H+L) Cross-Adsorbed Secondary Antibody, DyLight™ 550 (1:1000, # SA5-10027, Invitrogen). After washing two times with PBS, cells were incubated with DAPI (1:1000, #D9542, Sigma) for 10 min, and washed again with PBS. Finally, membranes were transferred on glass slides, embedded in ProLong Glass antifade mountant (#P36980, Invitrogen), and covered with a glass coverslip. Images were acquired using the confocal microscope Nikon eclipse Ti2 and analyzed with the NIS-Elements software (Nikon, v. 5.21.01).

4. RESULTS

4.1. PART 1

4.1.1. Characteristics of the study population

A complete descriptive analysis of the socio-demographic characteristics of the study population is reported in **Table 2**. Among the n=93 subjects randomly selected from the DeprAir study population, the mean age was 52.0 years and almost two thirds (63.4%) were females. More than half (52.7%) were normal weight, while 41.9% were overweight or obese, and 5.4% underweight. 78.5% held at least a high-school diploma, and 50.5% were employed at the time of recruitment. Most subjects were non-smokers, with 62.4% having never smoked and 8.6% being former smokers; besides, two thirds (66.7%) declared not to be exposed to secondhand smoke. Instead, the road traffic at residential address was moderate or heavy in most cases (72.1%). Regarding the mode of recruitment, 35.5% of study subjects were recruited during outpatient visits, 22.6% at day-hospitals, 7.5% were hospitalized, while 34.4% were former patients specifically recruited for the DeprAir study.

Table 2. Socio-demographic characteristics of the study population.

Socio-demographic characteristics	**Mean (SD) / N (%)**
Age (years)	52.0 (16.0)
Sex	
Females	59 (63.4%)
Males	34 (36.6%)
Body mass index (BMI; kg/m^2)	
Underweight (BMI<18,49)	5 (5.4%)
Normal weight (18,5<BMI<24,99)	49 (52.7%)
Overweight (25<BMI<29,99)	28 (30.1%)
Obese (BMI>30)	11 (11.8%)
Education	
Primary school	2 (2.2%)
Secondary school	18 (19.4%)
High school	41 (44.1%)
University degree	32 (34.4%)

Occupation	
Employed	47 (50.5%)
Unemployed	22 (23.7%)
Retired	19 (20.4%)
Other	5 (5.4%)
Smoking status	
Never smoked	58 (62.4%)
Former smoker	8 (8.6%)
Current smoker	27 (29.0%)
Secondhand smoking exposure	
Yes	31 (33.3%)
No	62 (66.7%)
Residence traffic exposure	
Mild	26 (28.0%)
Moderate	29 (31.2%)
Heavy	38 (40.9%)
Source of recruitment	
Outpatients	33 (35.5%)
Day-hospital	21 (22.6%)
Hospitalizations	7 (7.5%)
Former patients recruited for the study	32 (34.4%)

The clinical characteristics of MDD for our study population are reported in **Table 3**. On average, the age of onset was 41.2 years, with 2.8 episodes of MDD experienced along lifetime. Most study participants had neither a family history of psychiatric disorders (58.1%), nor of MDD (68.8%). The majority did not have psychotic symptoms (94.6%), did not try to commit suicide (86.0%), and did not suffer from seasonal depression (67.7%). The most prevalent MDD subtypes were the melancholic (31.2%) and the one with marked symptoms of anxiety (43.0%), with the rest having atypical (18.3%), psychotic (1.1%) or no prevalent type of MDD (6.5%). Among substance abusers (20.4%), alcohol and cannabis were the most common types of abuse. Most subjects (91.4%) were under antidepressant treatment at the time of recruitment, with 58.8% taking Selective Serotonin Reuptake Inhibitors (SSRI).

Table 3. Major Depressive Disorder (MDD) characteristics of the 93 study participants.

Major Depressive Disorder (MDD) characteristics	**Mean (SD) / N (%)**
Age at onset of MDD (years)	41.2 (17.7)
Number of MDD episodes	2.8 (3.0)
Family history of psychiatric disorders	
Yes	39 (41.9%)
No	54 (58.1%)
Family history of MDD	
Yes	29 (31.2%)
No	64 (68.8%)
Total duration of untreated MDD (months)	22.9 (46.7)
Total duration of MDD (years)	10.4 (12.6)
Duration of the last MDD episode (months)	11.0 (15.1)
Hospitalization for MDD	
Yes	20 (21.5%)
No	73 (78.5%)
Among those hospitalized for MDD (20), number of hospitalizations	1.3 (0.6)
Psychotic symptoms	
Yes	5 (5.4%)
No	88 (94.6%)
Suicide attempts	
Yes	13 (14.0%)
No	80 (86.0%)
Seasonality of MDD	
Yes	30 (32.3%)
No	63 (67.7%)
MDD subtype	
Melancholic	29 (31.2%)
Atypical	17 (18.3%)
Psychotic	1 (1.1%)
Marked symptoms of anxiety	40 (43.0%)
No prevalent type	6 (6.5%)
Lifetime substance abuse	
Single abuse	17 (18.3%)

Multiple abuse	2 (2.1%)
No	74 (79.6%)
Among abusers (n=19), type(s) of abuse	
Alcohol	7 (36.8%)
Cannabis	10 (52.6%)
Heroine	1 (5.3%)
Cocaine	2 (10.5%)
LSD	0 (0.0%)
Amphetamine	0 (0.0%)
3,4-methylenedioxymethamphetamine (MDMA)	0 (0.0%)
Drugs	4 (21.1%)
Currently under treatment with antidepressants	
Yes	85 (91.4%)
No	8 (8.6%)
Type of treatment	
Selective Serotonin Reuptake Inhibitors (SSRI)	50 (58.8%)
Serotonin and Norepinephrine Reuptake Inhibitors (SNRI)	10 (11.7%)
Tricyclics	10 (11.7%)
Bupropion	0 (0.0%)
Mirtazapine	4 (4.7%)
Vortioxetine	2 (2.4%)
Trazodone	4 (4.7%)
Others	5 (5.9%)

MDD severity measured according to the 5 rating scales considered is reported in **Table 4**. Based on the MADRS scale, the average score was 26.9, which falls into the range of moderate depression (20-34). According to the HAM-D scale, the average score was 23.1, which falls between moderate (17-23) and severe depression (≥24). The mean GAF score was 60.4 (moderate impairment of functioning); similarly, most subjects (55.9%) were classified as moderately or markedly ill according to the CGI scale. Finally, the subdomains of the SDS scale investigating the social, domestic and working impairment due to MDD returned average scores above 6 (out of 10); analogous results were found for the perceived stress category. The average score for the perceived social support was 62.5 (out of 100).

Table 4. Depressive Disorder (MDD) severity of the 93 study participants, as measured by different rating scales.

MDD severity	**Mean (SD) / N (%)**
Montgomery-Asberg Depression Rating Scale (MADRS; 0-60)	26.9 (11.6)
Hamilton Depression Rating Scale (HAM-D; 0-67)	23.1 (10.0)
Global Assessment of Functioning (GAF; 100-0)	60.4 (13.4)
Clinical Global Impression (CGI)	
Not at all ill	3 (3.2%)
Borderline mentally ill	14 (15.1%)
Mildly ill	18 (19.4%)
Moderately ill	31 (33.3%)
Markedly ill	21 (22.6%)
Severely ill	5 (5.4%)
Extremely ill	1 (1.1%)
Sheehan Disability Scale (SDS)	
Impairment at work/ school (0-10)	7.5 (2.3)
Impairment in relationships/ social life (0-10)	7.1 (2.1)
Impairment in family life/ home responsibilities (0-10)	6.9 (2.4)
Perceived stress (0-10)	6.8 (2.5)
Perceived social support (100-0)	62.5 (25.0)

Concerning exposure to air pollutants at the time points/lags considered, results are reported in **Table 5**. For $PM_{2.5}$, the mean exposure was 17.3 μg/m^3 for day 0, and 15.3 μg/m^3 for day -1. Regarding long-term exposure to $PM_{2.5}$, the average values were 21.8 and 21.2 μg/m^3 for the 6 months (lag 0-180) and for the year (lag 0-365) preceding blood sampling, respectively. For NO_2, the mean exposure was 37.0 μg/m^3 for day 0, 35.6 μg/m^3 for day -1, 37.1 μg/m^3 at lag 0-180, and 36.8 μg/m^3 in the year preceding blood sampling.

Table 5. Exposure to air pollutants of the study participants.

Air pollutants		**Mean exposure (SD)**		
	Day 0	*Day -1*	*Lag 0-180*	*Lag 0-365*
$PM_{2.5}$ (μg/m^3)	17.3 (11.6)	15.3 (9.6)	21.8 (7.2)	21.2 (1.6)

NO_2 (μg/m^3)	37.0 (14.6)	35.6 (14.1)	37.1 (9.9)	36.8 (4.0)

4.1.2. Characteristics of neuron-derived EVs

To validate the efficacy of the immunocapture protocol, L1CAM+ EVs derived from plasma pools of healthy donors were analyzed by flow cytometry before (total plasma EVs) and after immunocapture. As shown in **Figure 6**, immunocaptured EVs were highly enriched in L1CAM+ EVs (more than 90.0%, on average) if compared to the starting material; accordingly, depletion of L1CAM+ EVs (i.e., all EVs that did not bind to the biotinylated antibody-streptavidin bead complex) was observed in the supernatant fraction.

Figure 6. Validation of L1CAM+ EVs immunocapture by flow cytometry. Panel A: Pre-IC= pre-immunocapture; Panel B and C: post-IC= post-immunocapture.

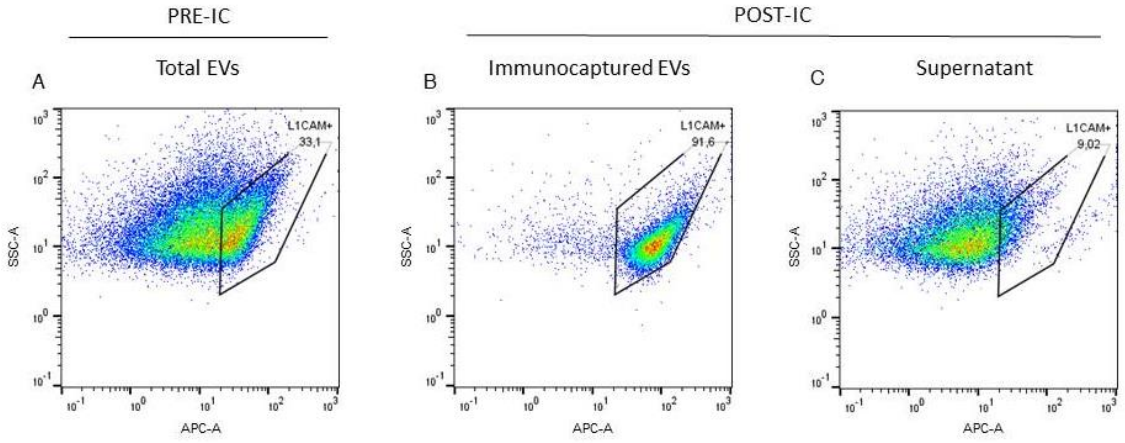

Plasma NdEVs (pools from healthy donors) were further characterized by NTA, in order to evaluate the concentration and size distribution of NdEVs compared to total plasma EVs. Only particles ranging from 30 nm to 700 nm were included in the analysis. As shown in **Figure 7**, the mean concentration of NdEVs was 1.9±1.0 $\times 10^6$ particles/ml, corresponding to 4.5% of total EVs (4.3±1.3 $\times 10^7$ particles/ml). Besides, NdEVs were on average smaller (mean size= 182±9 nm; min= 173 nm; max= 192 nm) than total EVs (mean size= 218±12 nm; min= 205 nm; max=229 nm) (**Figure 8**).

Figure 7. NdEV analysis by NTA. Concentration of NdEVs vs total EVs.

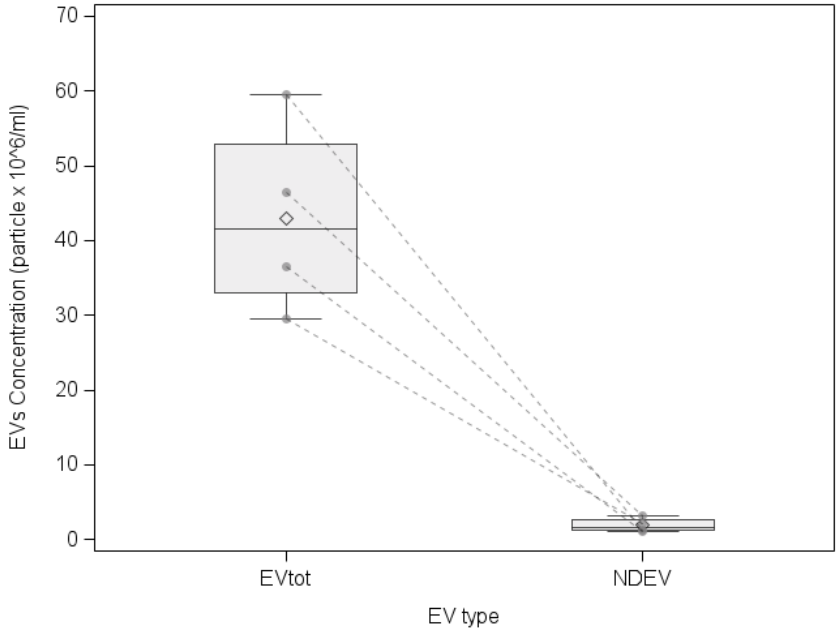

Figure 8. NdEV analysis by NTA. Size distribution (30-700 nm) of NdEVs vs total EVs. Total EVs are displayed in blue, NdEVs in green.

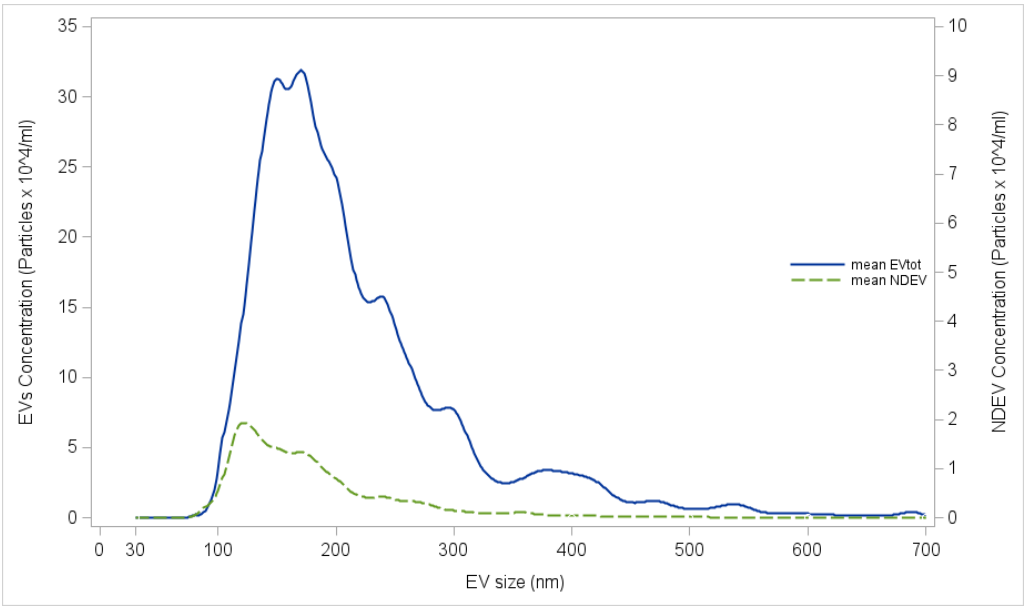

4.1.3. Preliminary screening of the miRNA content of plasma NdEVs

A preliminary screening of the miRNA content of plasma NdEVs was conducted on three pools of healthy donors and three pools of subjects with MDD; for each pool, total

EVs and NdEVs were analyzed. The quality of miRNAs extracted from NdEVs was assessed by Bioanalyzer (**Figure 9**), which shows a peak around 20-25 s, as expected.

Figure 9. Quality of extracted miRNAs. The arrow indicates the miRNA peak.

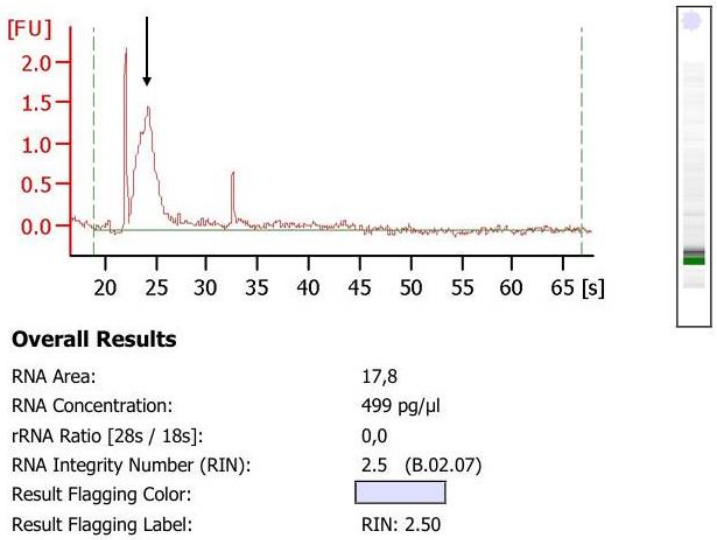

Of the 754 miRNAs measured, 512 (67.9%) were immediately excluded as they were not expressed in any sample. Of the remaining 242 miRNAs, 65 (26.9%) were found in at least one NdEV sample. In detail, 12 were detected in all NdEV samples, seven in five out of six NdEV samples, five in two thirds of NdEV samples, eight in half NdEV samples, nine in one third of NdEV samples, and 24 in only one NdEV sample out of six. Among the latter, miRNAs were screened out if detected in only one sample from healthy donors. U6 rRNA and ath-miR159a were chosen as endogenous/internal controls for data normalization (U6 rRNA was the best normalizer for NdEVs, ath-miR159a for total EVs). The 52 miRNAs selected through this screening are listed in **Table 6**. Of these miRNAs, 25 (48.1%) were overexpressed in NdEVs if compared to total EVs.

Table 6. List of 52 miRNA selected. For each miRNA, frequency in NdEVs and in total EVs, as well as fold-change (NdEVs vs total EVs) are indicated. Expression data for the calculation of fold-change were normalized with U6 rRNA.

miRNA	**Frequency in NdEVs**	**Frequency in total EVs**	**Fold-change (NdEVs vs total EVs)**

miR-1274B	6	6	1,30
miR-203	6	6	48,52
miR-218	6	5	26,80
miR-223	6	6	0,10
miR-24	6	6	0,13
miR-30a-5p	6	6	0,44
miR-30b	6	6	0,05
miR-320	6	6	0,36
miR-451	6	6	0,06
miR-572	6	6	42,09
miR-645	6	5	64,79
miR-92a	6	6	0,19
miR-133a	5	6	4,71
miR-150	5	6	0,02
miR-19b	5	6	0,20
miR-30c	5	6	0,05
miR-484	5	6	0,07
miR-601	5	5	2886,27
miR-638	5	6	19,30
miR-106b	4	6	0,12
miR-191	4	6	0,10
miR-212	4	3	17,86
miR-26b	4	6	0,26
miR-328	4	6	0,24
miR-125b	3	5	3,61
miR-126	3	6	0,04
miR-146a	3	6	0,03
miR-20a	3	6	0,05
miR-27a	3	6	2,12
miR-483-5p	3	6	514,05
miR-548a	3	2	36,14
miR-597	3	3	49,93
miR-127	2	6	2,58
miR-152	2	6	2,58
miR-193b	2	6	1,11

miR-206	2	1	65,05
miR-25	2	6	0,34
miR-28-3p	2	6	0,45
miR-30d	2	6	0,35
miR-331	2	6	0,11
miR-720	2	6	0,66
miR-142-3p	1	6	0,08
miR-181a	1	6	0,72
miR-184	1	3	26,28
miR-221	1	6	0,24
miR-222	1	6	0,06
miR-28	1	6	1,01
miR-29b	1	5	6,03
miR-323-3p	1	6	28,54
miR-520b	1	3	46,26
miR-520c-3p	1	0	51,28
miR-548b-5p	1	0	48,29

Also miR-124a-3p and miR-9-5p were added to the list as they are known to be neuron-specific miRNAs, according to both literature [79,80] and database search (miRNA Tissue Atlas database [81] and miTED database [82], see **Figure 10**).

Figure 10. Top-5 tissues expressing miR-124a-3p and miR-9-5p, based on miTED database (search terms: tissues, healthy status).

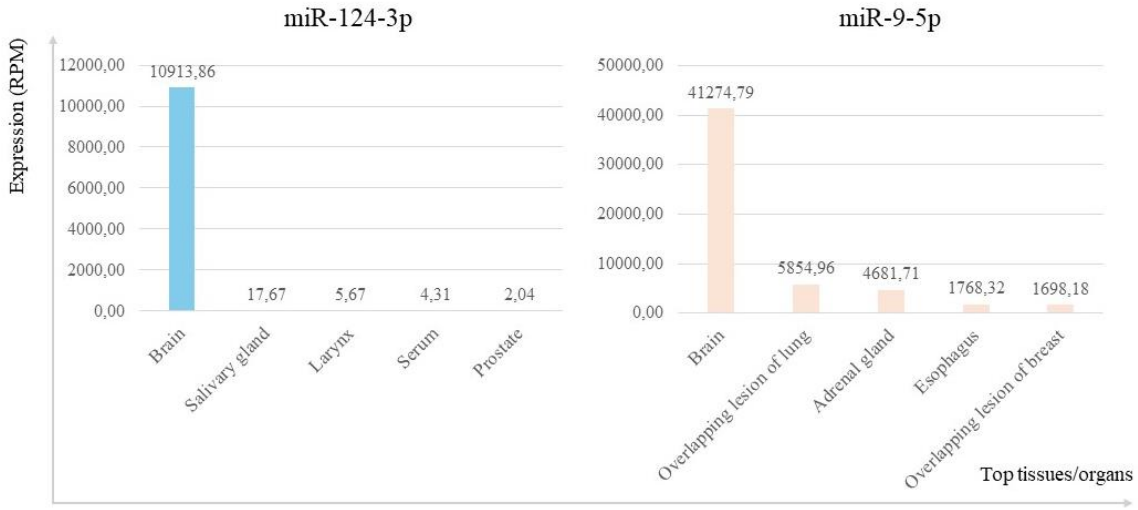

4.1.4. Target analysis and functional annotation of NdEV miRNAs

Target prediction and pathway analysis were carried out to functionally characterize the identified NdEV miRNAs. miR-1274B and miR-720 were excluded from the analysis as they are not *bona fide* miRNAs; indeed, they might derive from tRNA processing and their mechanisms of action is currently unknown [83]. Overall, the selected 50 miRNAs were found to target 128 validated genes (FDR p-value<0.01). The list of the top-10 genes regulated by such miRNAs is reported in **Table 7**. The genes regulated by the highest number of miRNAs were *TP53* (n=18 miRNAs), *KPNA6* (n=16 miRNAs), *PLAGL2* (n=15 miRNAs), *ARPP19* (n=14 miRNAs), *SLC7A11*(n=14 miRNAs), *PKM* (n=13 miRNAs), *TWF1*(n=13 miRNAs), *TNFRSF10B* (n=13 miRNAs), *FYCO1* (n=12 miRNAs), and *DNMT1*(n=12 miRNAs).

Table 7. Top-10 genes regulated by selected miRNAs.

Target gene	P-value	FDR p-value	Targeting miRNAs
TP53	1.68e-9	1.44e-5	miR-223-3p; miR-24-3p; miR-30a-5p; miR-30b-5p; miR-150-5p; miR-19b-3p; miR-30c-5p; miR-638; miR-106b-5p; miR-125b-5p; miR-20a-5p; miR-27a-3p; miR-25-3p; miR-28-3p; miR-30d-5p; miR-221-3p; miR-222-3p; miR-28-5p
KPNA6	6.82e-8	1.44e-4	miR-24-3p; miR-30a-5p; miR-30b-5p; miR-92a-3p; miR-133a-3p; miR-150-5p; miR-19b-3p; miR-30c-5p; miR-106b-5p; miR-26b-5p; miR-20a-5p; miR-30d-5p; miR-221-3p; miR-222-3p; miR-520b-3p; miR-520c-3p
PLAGL2	5.70e-5	0,0062569	miR-203a-3p; miR-24-3p; miR-30a-5p; miR-30b-5p; miR-30c-5p; miR-484; miR-106b-5p; miR-212-3p; miR-126-3p; miR-20a-5p; miR-27a-3p; miR-206; miR-30d-5p; miR-184; miR-548b-5p
ARPP19	1.50e-5	0,0029103	miR-203a-3p; miR-218-5p; miR-30a-5p; miR-30b-5p; miR-320a-3p; miR-451a; miR-92a-3p; miR-19b-3p; miR-30c-5p; miR-26b-5p; miR-548a-3p; miR-206; miR-28-3p; miR-30d-5p
SLC7A11	4.62e-6	0,0016465	miR-218-5p; miR-30a-5p; miR-92a-3p; miR-150-5p; miR-19b-3p; miR-106b-5p; miR-26b-5p; miR-20a-5p; miR-27a-3p; miR-25-3p; miR-142-3p; miR-181a-5p; miR-520b-3p; miR-520c-3p
PKM	8.16e-6	0,0021606	miR-218-5p; miR-30a-5p; miR-320a-3p; miR-92a-3p; miR-

			133a-3p; miR-19b-3p; miR-30c-5p; miR-484; miR-328-3p; miR-125b-5p; miR-184; miR-221-3p; miR-222-3p
TWF1	7.79e-7	4.76e-4	miR-223-3p; miR-30a-5p; miR-30b-5p; miR-92a-3p; miR-30c-5p; miR-106b-5p; miR-126-3p; miR-20a-5p; miR-193b-3p; miR-206; miR-25-3p; miR-30d-5p; miR-142-3p
TNFRSF10B	1.15e-4	0,0082884	miR-30a-5p; miR-30b-5p; miR-92a-3p; miR-19b-3p; miR-30c-5p; miR-106b-5p; miR-125b-5p; miR-20a-5p; miR-30d-5p; miR-331-3p; miR-323a-3p; miR-520b-3p; miR-520c-3p
FYCO1	1.01e-7	1.44e-4	miR-203a-3p; miR-218-5p; miR-30a-5p; miR-30b-5p; miR-92a-3p; miR-19b-3p; miR-30c-5p; miR-484; miR-106b-5p; miR-20a-5p; miR-30d-5p; miR-142-3p
DNMT1	2.47e-7	2.64e-4	miR-218-5p; miR-30a-5p; miR-30b-5p; miR-92a-3p; miR-19b-3p; miR-30c-5p; miR-484; miR-126-3p; miR-20a-5p; miR-152-3p; miR-193b-3p; miR-29b-3p

Among the top-biological processes regulated by the 52 miRNAs, intracellular signal transduction, cell response to stress/external cues, and immune and senescence-related processes were found to be enriched (if compared to the targets of the 754 miRNAs tested in the preliminary screening) (**Figure 11**).

Figure 11. Top biological processes regulated by selected miRNAs.

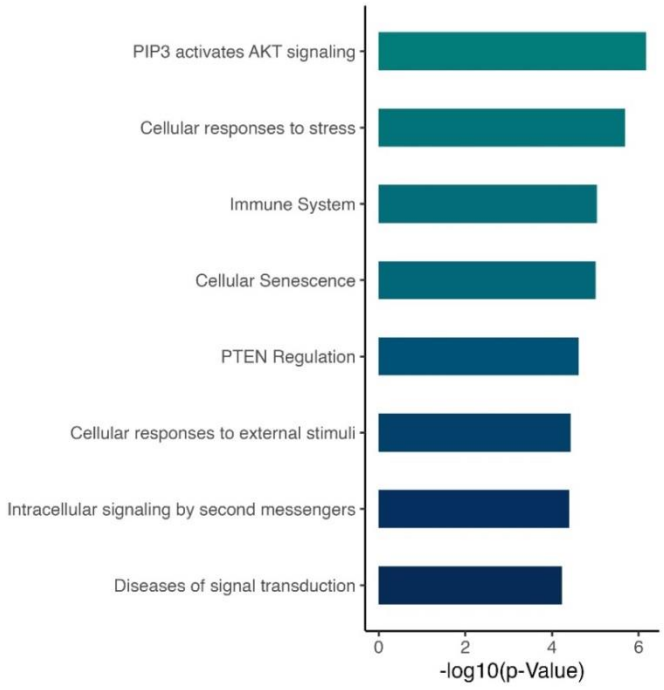

4.1.5. Association between air pollution exposure, NdEV miRNAs, and MDD severity

When considering the study population, only 17 miRNAs were included for statistical analysis as they were expressed in >70% subjects (**Table 8**).

Table 8. Percentage of expression of miRNAs in the study population.

miRNA	N. missing subjects	Percentage missing	Decision
miR-106b	71	74.74%	Excluded
miR-125b	41	43.16%	Excluded
miR-126	11	11.58%	Included
miR-127	90	94.74%	Excluded
miR-1274B	0	0.00%	Included
miR-133a	85	89.47%	Excluded
miR-142-3p	10	10.53%	Included
miR-146a	48	50.53%	Excluded
miR-150	79	83.16%	Excluded
miR-152	88	92.63%	Excluded
miR-181a	82	86.32%	Excluded
miR-191	23	24.21%	Included
miR-193b	46	48.42%	Excluded
miR-19b	5	5.26%	Included
miR-203	3	3.16%	Included
miR-206	70	73.68%	Excluded
miR-20a	58	61.05%	Excluded
miR-218	6	6.32%	Included
miR-221	87	91.58%	Excluded
miR-223	15	15.79%	Included
miR-24	10	10.53%	Included
miR-25	73	76.84%	Excluded
miR-26b	58	61.05%	Excluded
miR-27a	68	71.58%	Excluded
miR-28	92	96.84%	Excluded
miR-29b	92	96.84%	Excluded
miR-30a-5p	11	11.58%	Included
miR-30b	20	21.05%	Included

miR-30c	43	45.26%	Excluded
miR-30d	70	73.68%	Excluded
miR-320	10	10.53%	Included
miR- 323_3p	94	98.95%	Excluded
miR-328	59	62.11%	Excluded
miR-331	79	83.16%	Excluded
miR-483_5p	64	67.37%	Excluded
miR-484	76	80.00%	Excluded
miR-520b	77	81.05%	Excluded
miR-520c_3p	91	95.79%	Excluded
miR-548a	94	98.95%	Excluded
miR-572	7	7.37%	Included
miR-601	81	85.26%	Excluded
miR-638	1	1.05%	Included
miR-720	1	1.05%	Included
miR-9	68	71.58%	Excluded
miR-92a	25	26.32%	Included
miR-124a	84	88.42%	Excluded
miR-451	26	27.37%	Included

Although brain-enriched miR-9 and miR-124a were under the inclusion threshold (with a percentage of missing of 71.58% and 88.42%, respectively), they showed a high correlation (Pearson correlation coefficient=0.78) as expected for miRNAs with similar organ-specific expression patterns, further supporting the efficiency of NdEV enrichment over total EVs.

Regarding miRNAs selected for analysis, we did not observe any association with short-term (day 0, day -1) or annual (lag 0-365) $PM_{2.5}$ exposure; however, the mean exposure for the 6 months preceding blood drawing (lag 0-180) was positively associated with miR-19b (β=2.25; 95% CI= 0.28; 4.22; p-value= 0.026) (**Tables 9-12**). Instead, NO_2 exposure was associated with increased levels of miR-1274B (β= 0.29; 95% CI= 0.01; 0.58; p-value= 0.044), miR-320 (β= 0.42; 95% CI= 0.03; 0.81; p-value= 0.033), miR-720 (β= 0.27; 95% CI= 0.01; 0.53; p-value= 0.039), and miR-451 (β= 0.75; 95% CI= 0.17; 1.33; p-value= 0.012) at day-1; and with increased levels of miR-19b (β= 1.00;

95% CI= 0.13; 1.88; p-value= 0.026) at lag 0-180 (**Tables 13-16**). Significant associations between air pollutants and NdEV miRNAs are summarized in **Figure 12**.

Figure 12. Associations between $PM_{2.5}$ or NO_2 exposures and NdEV miRNAs. Only time points/lags with significant associations are displayed.

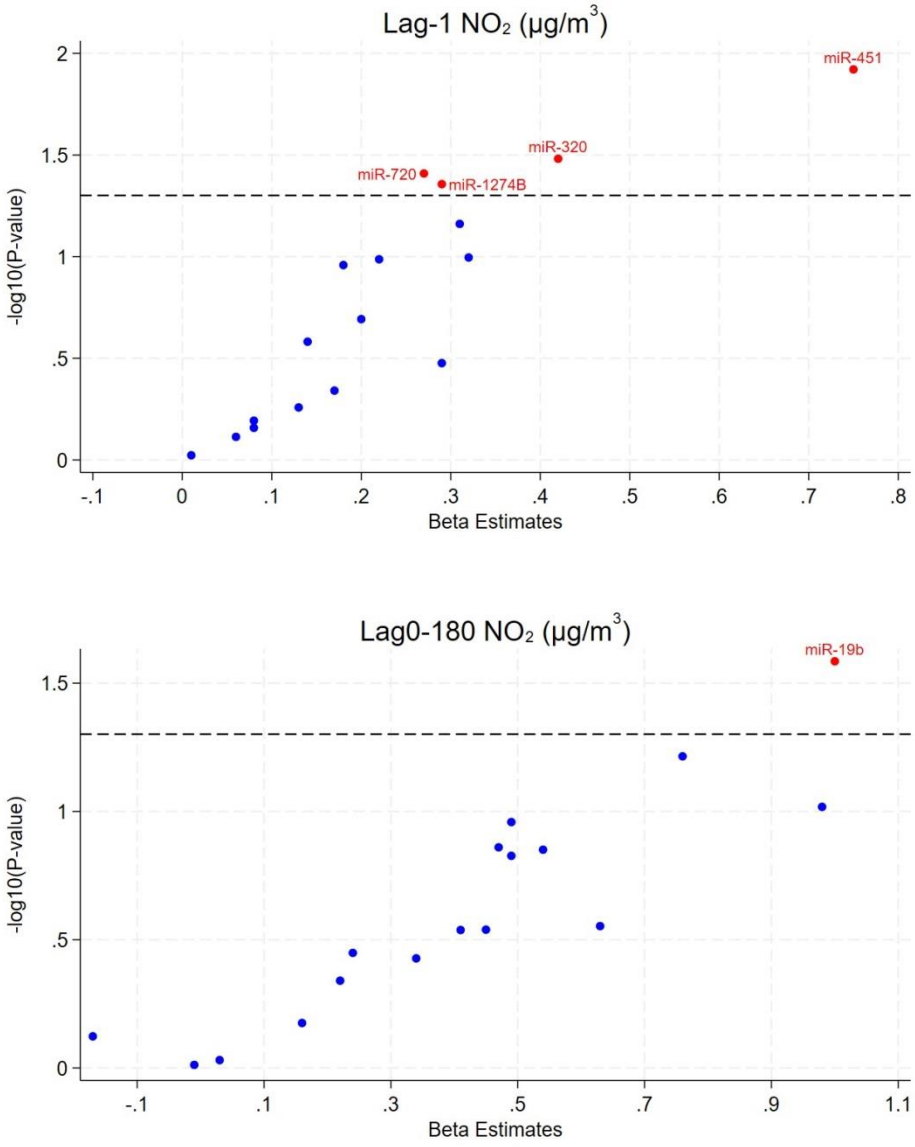

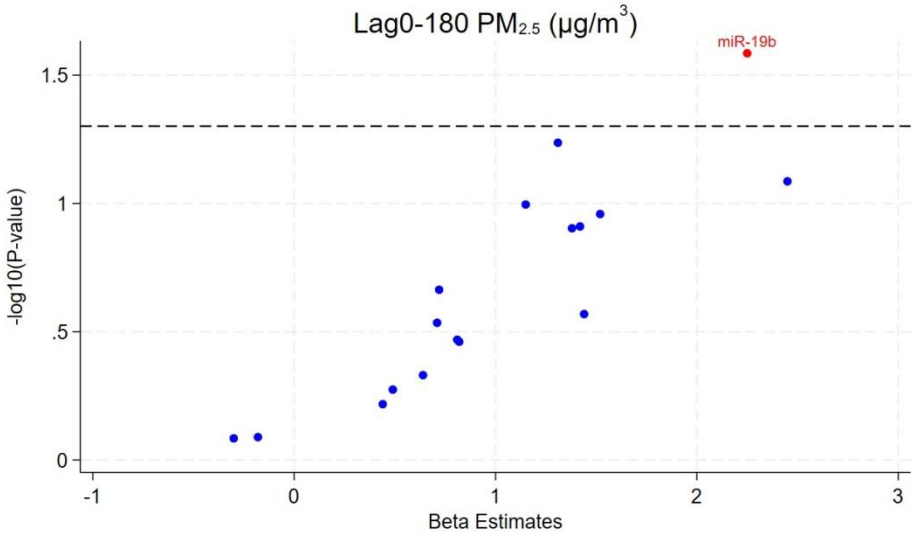

Table 9. Association between $PM_{2.5}$ exposure (increments of 10 µg/ m^3) at day 0 and miRNA levels. Significant associations (p-value<0.05; FDR p-value<0.100) are highlighted in bold.

miRNA	**β estimate**	**95% CI**	**p-value**	**FDR p-value**
miR-126	-0.14	-0.63; 0.36	0.575	0.961
miR-1274B	0.14	-0.20; 0.48	0.681	0.961
miR-142-3p	0.05	-0.35; 0.46	0.802	0.961
miR-191	-0.11	-0.71; 0.48	0.708	0.961
miR-19b	-0.05	-0.50; 0.39	0.808	0.961
miR-203	0.27	-0.09; 0.63	0.141	0.961
miR-218	0.16	-0.15; 0.46	0.310	0.961
miR-223	-0.08	-0.50; 0.33	0.697	0.961
miR-24	-0.12	-0.52; 0.29	0.559	0.961
miR-30a-5p	-0.03	-0.42; 0.36	0.866	0.961
miR-30b	0.03	-0.43; 0.50	0.884	0.961
miR-320	-0.11	-0.54; 0.31	0.596	0.961
miR-572	0.12	-0.20; 0.43	0.458	0.961
miR-638	0.00	-0.25; 0.26	0.970	0.970
miR-720	0.17	-0.13; 0.48	0.257	0.961
miR-92a	0.03	-0.53; 0.59	0.904	0.961
miR-451	0.08	-0.54; 0.70	0.793	0.961

Table 10. Association between $PM_{2.5}$ exposure (increments of 10 μg/ m^3) at day -1 and miRNA levels. Significant associations (p-value<0.05; FDR p-value<0.100) are highlighted in bold.

miRNA	β estimate	95% CI	p-value	FDR p-value
miR-126	0.12	-0.37; 0.60	0.629	0.783
miR-1274B	0.25	-0.09; 0.60	0.150	0.703
miR-142-3p	0.04	-0.38; 0.46	0.862	0.927
miR-191	0.14	-0.46; 0.74	0.645	0.783
miR-19b	0.25	-0.22; 0.73	0.290	0.703
miR-203	0.19	-0.20; 0.57	0.331	0.703
miR-218	0.20	-0.11; 0.51	0.198	0.703
miR-223	-0.11	-0.55; 0.32	0.606	0.783
miR-24	0.02	-0.40; 0.44	0.927	0.927
miR-30a-5p	-0.11	-0.50; 0.28	0.588	0.783
miR-30b	-0.03	-0.52; 0.46	0.909	0.927
miR-320	0.26	-0.20; 0.72	0.269	0.703
miR-572	0.09	-0.22; 0.40	0.562	0.783
miR-638	0.10	-0.16; 0.37	0.436	0.783
miR-720	0.18	-0.14; 0.49	0.269	0.703
miR-92a	0.31	-0.31; 0.92	0.322	0.703
miR-451	0.51	-0.15; 1.18	0.128	0.703

Table 11. Association between $PM_{2.5}$ exposure (increments of 10 μg/ m^3) at lag 0-180 and miRNA levels. Significant associations (p-value<0.05; FDR p-value<0.100) are highlighted in bold.

miRNA	β estimate	95% CI	p-value	FDR p-value
miR-126	1.52	-0.35; 3.40	0.110	0.304
miR-1274B	0.49	-1.07; 2.05	0.532	0.646
miR-142-3p	0.82	-0.91; 2.56	0.346	0.490
miR-191	-0.30	-3.01; 2.41	0.824	0.824
miR-19b	**2.25**	**0.28; 4.22**	**0.026**	0.304
miR-203	0.44	-1.25; 2.12	0.606	0.687
miR-218	0.71	-0.63; 2.05	0.292	0.490

miR-223	0.64	-1.12; 2.40	0.467	0.611
miR-24	0.81	-0.87; 2.49	0.340	0.490
miR-30a-5p	-0.18	-1.75; 1.38	0.815	0.824
miR-30b	1.38	-0.40; 3.16	0.125	0.304
miR-320	1.42	-0.39; 3.23	0.123	0.304
miR-572	1.15	-0.23; 2.54	0.101	0.304
miR-638	0.72	-0.44; 1.89	0.217	0.461
miR-720	1.31	-0.04; 2.66	0.058	0.304
miR-92a	1.44	-1.16; 4.04	0.270	0.490
miR-451	2.45	-0.32; 5.23	0.082	0.304

Table 12. Association between $PM_{2.5}$ exposure (increments of 10 μg/ m^3) at lag 0-365 and miRNA levels. Significant associations (p-value<0.05; FDR p-value<0.100) are highlighted in bold.

miRNA	**β estimate**	**95% CI**	**p-value**	**FDR p-value**
miR-126	-0.37	-3.23; 2.50	0.799	0.945
miR-1274B	0.18	-2.07; 2.43	0.873	0.945
miR-142-3p	0.16	-2.34; 2.67	0.897	0.945
miR-191	0.22	-3.43; 3.88	0.902	0.945
miR-19b	1.62	-1.34; 4.57	0.279	0.945
miR-203	0.46	-1.91; 2.83	0.700	0.945
miR-218	0.25	-1.65; 2.14	0.795	0.945
miR-223	1.57	-0.89; 4.03	0.205	0.945
miR-24	-0.11	-2.68; 2.45	0.930	0.945
miR-30a-5p	0.14	-1.99; 2.26	0.897	0.945
miR-30b	1.60	-0.91; 4.11	0.206	0.945
miR-320	0.19	-2.47; 2.85	0.885	0.945
miR-572	0.84	-1.21; 2.89	0.416	0.945
miR-638	-0.13	-1.82; 1.57	0.880	0.945
miR-720	0.47	-1.54; 2.48	0.643	0.945
miR-92a	0.43	-3.07; 3.93	0.806	0.945
miR-451	0.13	-3.60; 3.86	0.945	0.945

Table 13. Association between NO_2 exposure (increments of 10 µg/ m^3) at day 0 and miRNA levels. Significant associations (p-value<0.05; FDR p-value<0.100) are highlighted in bold.

miRNA	β estimate	95% CI	p-value	FDR p-value
miR-126	-0.09	-0.55; 0.38	0.714	0.847
miR-1274B	0.22	-0.11; 0.55	0.181	0.847
miR-142-3p	0.09	-0.31; 0.49	0.664	0.847
miR-191	-0.15	-0.69; 0.39	0.572	0.847
miR-19b	0.25	-0.19; 0.69	0.259	0.847
miR-203	0.15	-0.21; 0.51	0.409	0.847
miR-218	0.01	-0.27; 0.30	0.940	0.940
miR-223	-0.12	-0.56; 0.32	0.580	0.847
miR-24	-0.07	-0.46; 0.32	0.719	0.847
miR-30a-5p	0.02	-0.33; 0.37	0.908	0.940
miR-30b	0.14	-0.32; 0.61	0.538	0.847
miR-320	0.15	-0.28; 0.57	0.492	0.847
miR-572	0.09	-0.21; 0.39	0.551	0.847
miR-638	-0.06	-0.30; 0.19	0.653	0.847
miR-720	0.08	-0.22; 0.37	0.614	0.847
miR-92a	0.11	-0.55; 0.76	0.747	0.847
miR-451	0.26	0.43; 0.95	0.448	0.847

Table 14. Association between $PM_{2.5}$ exposure (increments of 10 µg/ m^3) at day -1 and miRNA levels. Significant associations (p-value<0.05; FDR p-value<0.100) are highlighted in bold.

miRNA	β estimate	95% CI	p-value	FDR p-value
miR-126	0.13	-0.30; 0.55	0.552	0.722
miR-1274B	**0.29**	**0.01; 0.58**	**0.044**	0.187
miR-142-3p	0.31	-0.02; 0.64	0.069	0.234
miR-191	0.17	-0.29; 0.63	0.456	0.646
miR-19b	0.32	-0.06; 0.70	0.101	0.234
miR-203	0.20	-0.11; 0.52	0.203	0.383
miR-218	0.14	-0.11; 0.39	0.262	0.445

miR-223	0.01	-0.39; 0.42	0.948	0.948
miR-24	0.06	-0.34; 0.45	0.770	0.818
miR-30a-5p	0.08	-0.25; 0.40	0.641	0.778
miR-30b	0.08	-0.32; 0.47	0.695	0.788
miR-320	**0.42**	**0.03; 0.81**	**0.033**	0.187
miR-572	0.22	-0.05; 0.48	0.103	0.234
miR-638	0.18	-0.04; 0.39	0.110	0.234
miR-720	**0.27**	**0.01; 0.53**	**0.039**	0.187
miR-92a	0.29	-0.30; 0.87	0.334	0.516
miR-451	**0.75**	**0.17; 1.33**	**0.012**	0.187

Table 15. Association between NO_2 exposure (increments of 10 µg/ m^3) at lag 0-180 and miRNA levels. Significant associations (p-value<0.05; FDR p-value<0.100) are highlighted in bold.

miRNA	**β estimate**	**95% CI**	**p-value**	**FDR p-value**
miR-126	0.45	-0.40; 1.30	0.289	0.493
miR-1274B	0.49	-0.18; 1.17	0.149	0.362
miR-142-3p	0.41	-0.36; 1.18	0.290	0.493
miR-191	-0.17	-1.25; 0.91	0.753	0.853
miR-19b	**1.00**	**0.13; 1.88**	**0.026**	0.362
miR-203	0.16	-0.58; 0.90	0.668	0.811
miR-218	0.22	-0.37; 0.81	0.457	0.598
miR-223	0.34	-0.42; 1.09	0.374	0.530
miR-24	-0.01	-0.75; 0.73	0.973	0.973
miR-30a-5p	0.03	-0.62; 0.68	0.932	0.973
miR-30b	0.54	-0.19; 1.27	0.141	0.362
miR-320	0.76	-0.04; 1.56	0.061	0.362
miR-572	0.47	-0.15; 1.09	0.138	0.362
miR-638	0.24	-0.27; 0.75	0.356	0.530
miR-720	0.49	-0.11; 1.09	0.110	0.362
miR-92a	0.63	-0.53; 1.78	0.280	0.493
miR-451	0.98	-0.18; 2.13	0.096	0.362

Table 16. Association between NO_2 exposure (increments of 10 μg/ m^3) at lag0-365 and miRNA levels. Significant associations (p-value<0.05; FDR p-value<0.100) are highlighted in bold.

miRNA	β estimate	95% CI	p-value	FDR p-value
miR-126	0.18	-0.76; 0.75	0.749	0.839
miR-1274B	0.56	-0.20; 1.31	0.145	0.731
miR-142-3p	0.37	-0.51; 1.24	0.405	0.731
miR-191	-0.48	-1.72; 0.76	0.437	0.731
miR-19b	0.69	-0.31; 1.69	0.174	0.731
miR-203	0.11	-0.70; 0.92	0.790	0.839
miR-218	0.04	-0.63; 0.70	0.915	0.915
miR-223	0.49	-0.41; 1.39	0.277	0.731
miR-24	-0.20	-1.02; 0.62	0.628	0.839
miR-30a-5p	0.15	-0.58; 0.89	0.683	0.839
miR-30b	0.46	-0.43; 1.34	0.306	0.731
miR-320	0.55	-0.38; 1.48	0.241	0.731
miR-572	0.45	-0.25; 1.15	0.205	0.731
miR-638	0.09	-0.49; 0.67	0.755	0.839
miR-720	0.33	-0.36; 1.01	0.344	0.731
miR-92a	0.46	-0.82; 1.73	0.473	0.731
miR-451	0.53	-0.77; 1.84	0.416	0.731

Interestingly, multiple miRNAs were associated with MDD severity scales. In particular, miR-126 (β= -2.50; 95% CI= -4.72; -0.28; p-value= 0.028), miR-19b (β= -2.13; 95% CI= -4.03; -0.22; p-value= 0.029), miR-572 (β= -4.04; 95% CI= -6.65; -1.42; p-value= 0.003), and miR-638 (β= -3.50; 95% CI= -6.59; -0.41; p-value= 0.027) were negatively associated with MADRS score (**Table 17**), while increments of miR-218 (β= -2.57; 95% CI= -4.83; -0.30; p-value= 0.027) and miR-572 (β= -2.64; 95% CI= -4.85; -0.43; p-value= 0.020) were associated with lower HAM-D scores (**Table 18**).

Besides, increasing levels of 8 miRNAs, i.e. miR-126 (β= 3.23; 95% CI= 0.90; 5.55; p-value= 0.007), miR-142-3p (β= 2.94; 95% CI= 0.23; 5.64; p-value= 0.034), miR-19b (β= 2.47; 95% CI= 0.29; 4.66; p-value= 0.027), miR-24 (β= 3.02; 95% CI= 0.11; 5.93; p-value= 0.042), miR-30a-5p (β= 3.33; 95% CI= 0.01; 6.65; p-value= 0.049), miR-30b

(β= 3.09; 95% CI= 0.06; 6.11; p-value= 0.046), miR-638 (β= 3.63; 95% CI= 0.03; 7.23; p-value= 0.048), and miR-451(β= 2.49; 95% CI= 0.22; 4.77; p-value= 0.032), were associated with better functioning, as indicated by higher GAF scores (**Table 19**).

In addition, 8 miRNAs, i.e. miR-126 (β= -0.79; 95% CI= -1.23; -0.36; p-value= ≤0.001), miR-142-3p (β= -0.55; 95% CI= -0.97; -0.12; p-value= 0.011), miR-19b (β= -0.37; 95% CI= -0.70; -0.05; p-value= 0.025), miR-218 (β= -0.65; 95% CI= -1.16; -0.15; p-value= 0.011), miR-30b (β= -0.62; 95% CI= -1.15; -0.10; p-value= 0.020), miR-572 (β= -0.76; 95% CI= -1.26; -0.26; p-value= 0.003), miR-638 (β= -0.92; 95% CI= -1.50; -0.34; p-value= 0.002), and miR-451(β= -0.55; 95% CI= -0.92; -0.17; p-value= 0.004) were associated with CGI scores (**Table 20**). Finally, miR-126 was found to be negatively associated with the disability - impairment at work (β= -0.52; 95% CI= -1.03; 0.00; p-value= 0.048) and home relationship (β= -0.49; 95% CI= -0.83; -0.15; p-value= 0.005) domains of the SDS scale; similarly, increasing miR-638 (β= -0.79; 95% CI= -1.54; -0.04; p-value= 0.041) was associated with decreasing scores in the disability - impairment at work domain of the SDS scale (**Tables 21-22**). Instead, no associations were found between NdEV miRNAs and the family responsibilities, perceived stress, and perceived social support domains of the SDS scale (**Tables 23-25**).

Significant associations between NdEV miRNAs and MDD severity scales are summarized in **Figure 13**.

Figure 13. Associations between NdEV miRNAs are MDD severity scales. Only scales with significant associations are displayed.

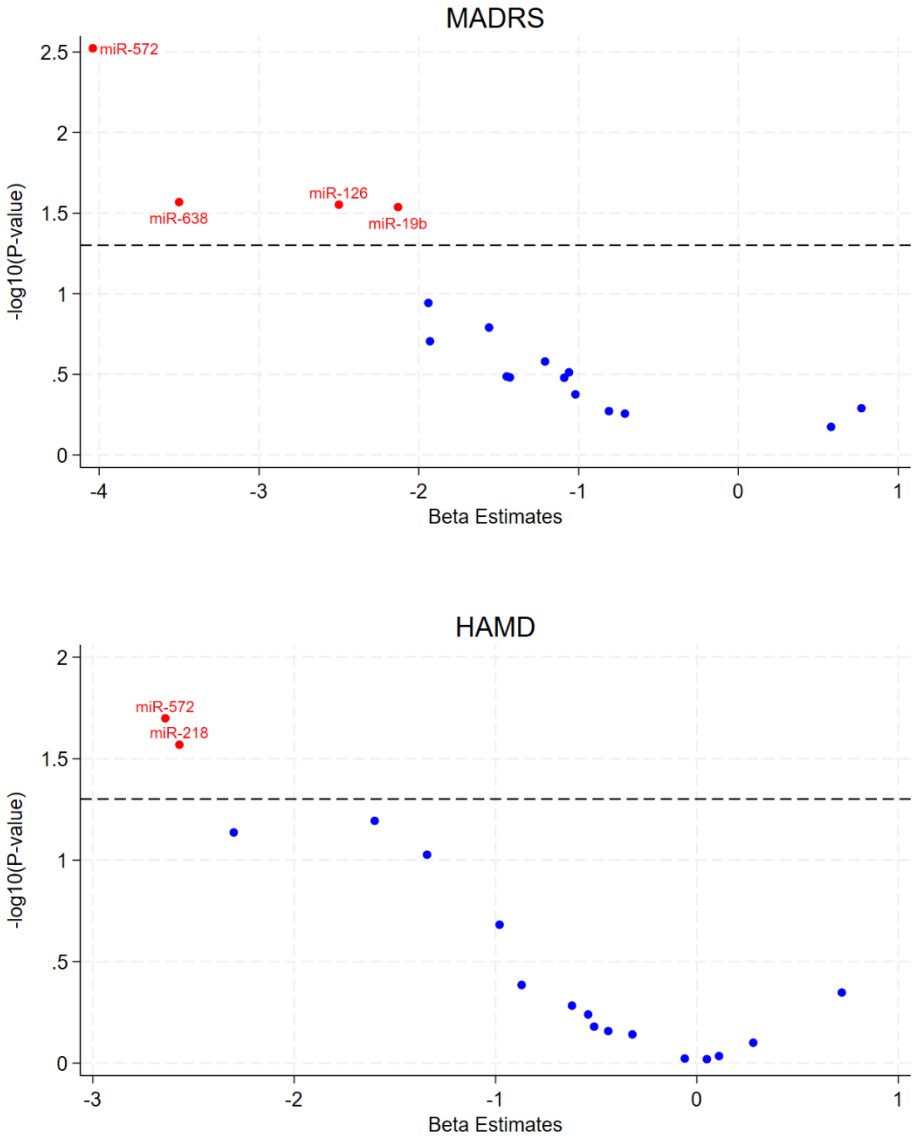

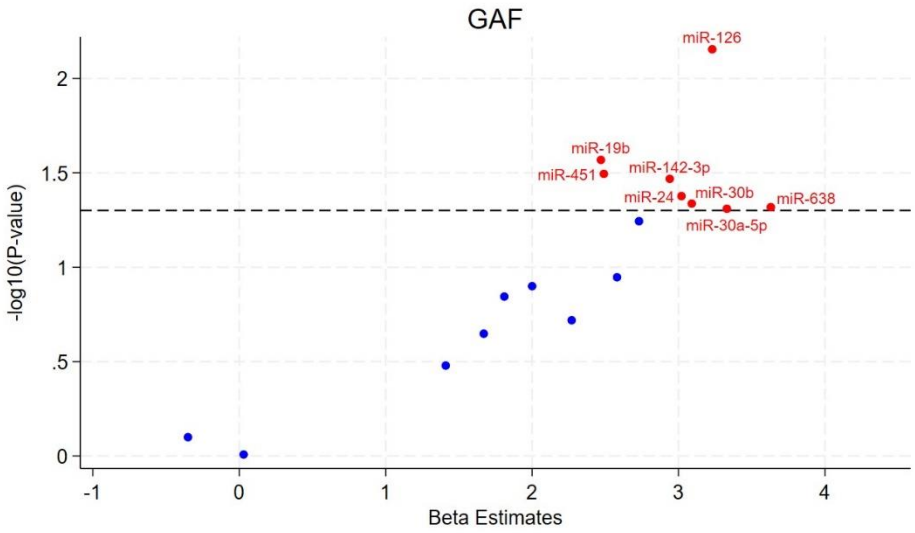
GAF
miR-126
miR-19b
miR-451
miR-142-3p
miR-24
miR-30b
miR-638
miR-30a-5p
-log10(P-value)
Beta Estimates

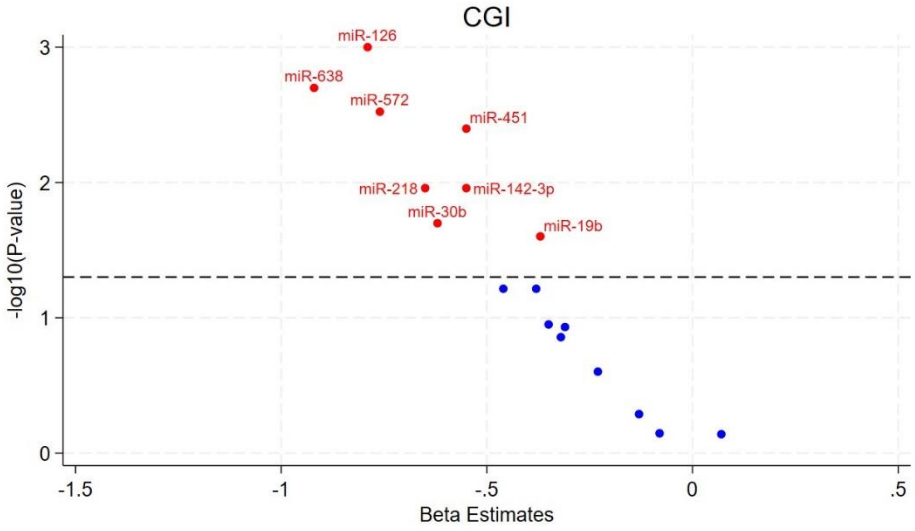
CGI
miR-126
miR-638
miR-572
miR-451
miR-218
miR-142-3p
miR-30b
miR-19b
-log10(P-value)
Beta Estimates

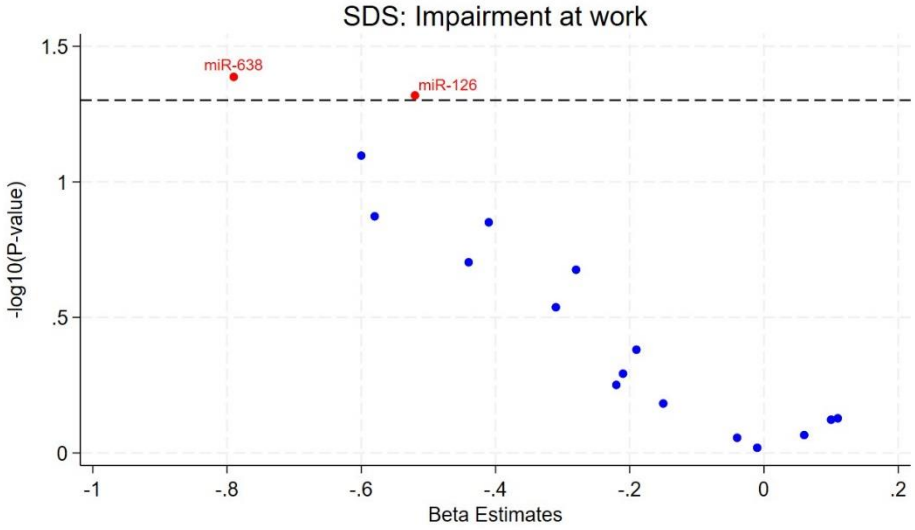
SDS: Impairment at work
miR-638
miR-126
-log10(P-value)
Beta Estimates

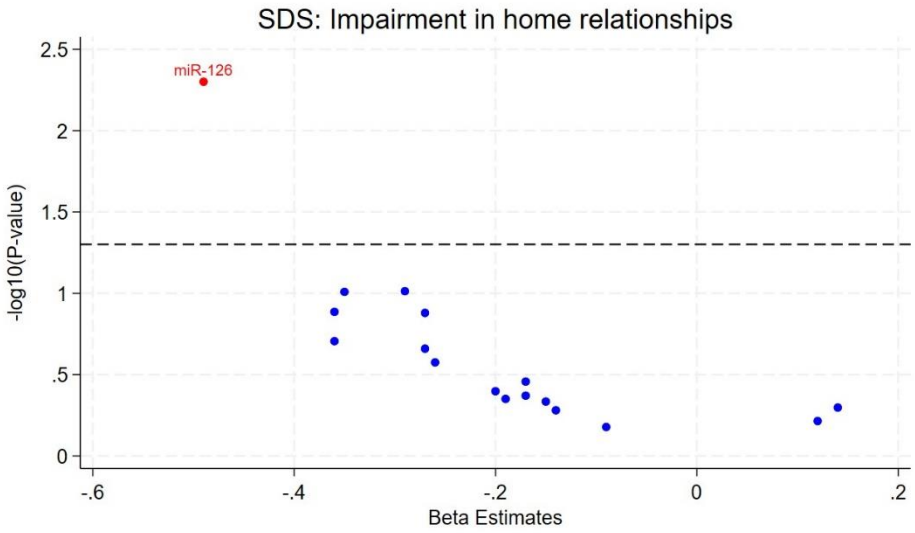

Table 17. Association between miRNA levels and MADRS scores. Significant associations (p-value<0.05; FDR p-value<0.100) are highlighted in bold.

miRNA	**β estimate**	**95% CI**	**p-value**	**FDR p-value**
miR-126	**-2.50**	**-4.72; -0.28**	**0.028**	0.123
miR-1274B	-0.71	-3.10; 1.68	0.554	0.589
miR-142-3p	-1.94	-4.36; 0.48	0.114	0.388
miR-191	-1.21	-3.36; 0.94	0.263	0.470
miR-19b	**-2.13**	**-4.03; -0.22**	**0.029**	0.123
miR-203	0.77	-1.56; 3.10	0.513	0.589
miR-218	-1.93	-4.89; 1.03	0.197	0.470
miR-223	-0.81	-3.40; 1.79	0.535	0.589
miR-24	-1.02	-3.55; 1.51	0.421	0.551
miR-30a-5p	-1.43	-4.34; 1.49	0.330	0.470
miR-30b	-1.45	-4.39; 1.49	0.326	0.470
miR-320	-1.56	-3.77; 0.65	0.162	0.459
miR-572	**-4.04**	**-6.65; -1.42**	**0.003**	**0.051**
miR-638	**-3.50**	**-6.59; -0.41**	**0.027**	0.123
miR-720	0.58	-2.13; 3.30	0.670	0.670
miR-92a	-1.09	-3.32; 1.15	0.332	0.470
miR-451	-1.06	-3.12; 1.01	0.307	0.470

Table 18. Association between miRNA levels and HAM-D scores. Significant associations (p-value<0.05; FDR p-value<0.100) are highlighted in bold.

miRNA	β estimate	95% CI	p-value	FDR p-value
miR-126	-1.60	-3.29; 0.09	0.064	0.310
miR-1274B	-0.54	-2.48; 1.39	0.576	0.944
miR-142-3p	-0.62	-2.55; 1.31	0.521	0.944
miR-191	-0.32	-2.10; 1.47	0.722	0.944
miR-19b	-1.34	-2.91; 0.23	0.094	0.320
miR-203	0.72	-1.17; 2.62	0.449	0.944
miR-218	**-2.57**	**-4.83; -0.30**	**0.027**	0.230
miR-223	0.28	-1.85; 2.41	0.793	0.956
miR-24	-0.87	-2.98; 1.24	0.412	0.944
miR-30a-5p	-0.51	-2.81; 1.80	0.661	0.944
miR-30b	-0.44	-2.66; 1.79	0.695	0.944
miR-320	-0.06	-1.87; 1.75	0.949	0.956
miR-572	**-2.64**	**-4.85; -0.43**	**0.020**	0.230
miR-638	-2.30	-4.82; 0.22	0.073	0.310
miR-720	0.11	-2.09; 2.31	0.923	0.956
miR-92a	0.05	-1.78; 1.88	0.956	0.956
miR-451	-0.98	-2.53; 0.57	0.208	0.589

Table 19. Association between miRNA levels and GAF scores. Significant associations (p-value<0.05; FDR p-value<0.100) are highlighted in bold.

miRNA	β estimate	95% CI	p-value	FDR p-value
miR-126	**3.23**	**0.90; 5.55**	**0.007**	0.104
miR-1274B	1.67	-1.05; 4.40	0.225	0.273
miR-142-3p	**2.94**	**0.23; 5.64**	**0.034**	0.104
miR-191	1.81	-0.64; 4.26	0.143	0.203
miR-19b	**2.47**	**0.29; 4.66**	**0.027**	0.104
miR-203	-0.35	-3.05; 2.34	0.795	0.845
miR-218	2.27	-1.16; 5.70	0.191	0.250
miR-223	2.73	-0.08; 5.54	0.057	0.108
miR-24	**3.02**	**0.11; 5.93**	**0.042**	0.104

miR-30a-5p	**3.33**	**0.01; 6.65**	**0.049**	0.104
miR-30b	**3.09**	**0.06; 6.11**	**0.046**	0.104
miR-320	2.00	-0.58; 4.57	0.126	0.195
miR-572	2.58	-0.63; 5.80	0.113	0.192
miR-638	**3.63**	**0.03; 7.23**	**0.048**	0.104
miR-720	0.03	-3.09; 3.16	0.983	0.983
miR-92a	1.41	-1.49; 4.30	0.332	0.376
miR-451	**2.49**	**0.22; 4.77**	**0.032**	0.104

Table 20. Association between miRNA levels and CGI scores. Significant associations (p-value<0.05; FDR p-value<0.100) are highlighted in bold.

miRNA	**β estimate**	**95% CI**	**p-value**	**FDR p-value**
miR-126	**-0.79**	**-1.23; -0.36**	**≤0.001**	**0.017**
miR-1274B	-0.38	-0.78; 0.02	0.061	0.104
miR-142-3p	**-0.55**	**-0.97; -0.12**	**0.011**	**0.031**
miR-191	-0.23	-0.61; 0.16	0.250	0.304
miR-19b	**-0.37**	**-0.70; -0.05**	**0.025**	**0.053**
miR-203	0.07	-0.32; 0.45	0.725	0.725
miR-218	**-0.65**	**-1.16; -0.15**	**0.011**	**0.031**
miR-223	-0.32	-0.74; 0.10	0.139	0.182
miR-24	-0.35	-0.79; 0.08	0.112	0.166
miR-30a-5p	-0.46	-0.93; 0.02	0.061	0.104
miR-30b	**-0.62**	**-1.15; -0.10**	**0.020**	**0.049**
miR-320	-0.31	-0.69; 0.08	0.117	0.166
miR-572	**-0.76**	**-1.26; -0.26**	**0.003**	**0.017**
miR-638	**-0.92**	**-1.50; -0.34**	**0.002**	**0.017**
miR-720	-0.08	-0.52; 0.36	0.714	0.725
miR-92a	-0.13	-0.50; 0.25	0.515	0.584
miR-451	**-0.55**	**-0.92; -0.17**	**0.004**	**0.017**

Table 21. Association between miRNA levels and SDS scores for the disability – impairment at work domain. Significant associations (p-value<0.05; FDR p-value<0.100) are highlighted in bold.

miRNA	β estimate	95% CI	p-value	FDR p-value
miR-126	**-0.52**	**-1.03; 0.00**	**0.048**	0.408
miR-1274B	-0.31	-0.90; 0.28	0.290	0.616
miR-142-3p	-0.41	-0.97; 0.14	0.141	0.479
miR-191	-0.28	-0.74; 0.17	0.211	0.512
miR-19b	-0.19	-0.66; 0.28	0.416	0.786
miR-203	-0.22	-0.97; 0.53	0.561	0.867
miR-218	-0.60	-1.28; 0.07	0.080	0.453
miR-223	0.06	-0.62; 0.74	0.859	0.934
miR-24	-0.15	-0.82; 0.52	0.657	0.916
miR-30a-5p	-0.58	-1.35; 0.19	0.134	0.479
miR-30b	0.10	-0.56; 0.76	0.754	0.916
miR-320	-0.01	-0.58; 0.55	0.957	0.957
miR-572	-0.44	-1.13; 0.24	0.198	0.512
miR-638	**-0.79**	**-1.54; -0.04**	**0.041**	0.408
miR-720	0.11	-0.55; 0.76	0.745	0.916
miR-92a	-0.04	-0.62; 0.54	0.879	0.934
miR-451	-0.21	-0.86; 0.44	0.510	0.867

Table 22. Association between miRNA levels and SDS scores for the home relationship domain. Significant associations (p-value<0.05; FDR p-value<0.100) are highlighted in bold.

miRNA	β estimate	95% CI	p-value	FDR p-value
miR-126	**-0.49**	**-0.83; -0.15**	**0.005**	**0.085**
miR-1274B	-0.09	-0.51; 0.33	0.664	0.664
miR-142-3p	-0.35	-0.77; 0.07	0.098	0.449
miR-191	-0.17	-0.53; 0.19	0.349	0.594
miR-19b	-0.29	-0.62; 0.05	0.097	0.449
miR-203	0.14	-0.27; 0.55	0.504	0.594
miR-218	-0.19	-0.70; 0.32	0.446	0.594

miR-223	-0.14	-0.59; 0.30	0.524	0.594
miR-24	-0.27	-0.70; 0.17	0.219	0.532
miR-30a-5p	-0.20	-0.68; 0.28	0.400	0.594
miR-30b	-0.26	-0.73; 0.21	0.266	0.565
miR-320	-0.15	-0.55; 0.26	0.463	0.594
miR-572	-0.36	-0.84; 0.11	0.130	0.449
miR-638	-0.36	-0.91; 0.19	0.197	0.532
miR-720	0.12	-0.35; 0.59	0.610	0.648
miR-92a	-0.17	-0.58; 0.25	0.426	0.594
miR-451	-0.27	-0.62; 0.08	0.132	0.449

Table 23. Association between miRNA levels and SDS scores for the family responsibilities domain. Significant associations (p-value<0.05; FDR p-value<0.100) are highlighted in bold.

miRNA	**β estimate**	**95% CI**	**p-value**	**FDR p-value**
miR-126	-0.32	-0.77; 0.13	0.157	0.887
miR-1274B	0.00	-0.50; 0.51	0.989	0.989
miR-142-3p	-0.33	-0.85; 0.18	0.203	0.887
miR-191	-0.11	-0.55; 0.34	0.635	0.900
miR-19b	-0.12	-0.52; 0.29	0.572	0.900
miR-203	0.32	-0.17; 0.81	0.198	0.887
miR-218	0.14	-0.48; 0.76	0.652	0.900
miR-223	-0.12	-0.64; 0.40	0.649	0.900
miR-24	-0.32	-0.81; 0.18	0.210	0.887
miR-30a-5p	-0.20	-0.76; 0.35	0.463	0.900
miR-30b	-0.04	-0.58; 0.51	0.892	0.948
miR-320	-0.10	-0.59; 0.38	0.676	0.900
miR-572	-0.10	-0.69; 0.49	0.732	0.900
miR-638	-0.09	-0.77; 0.59	0.794	0.900
miR-720	0.17	-0.40; 0.74	0.554	0.900
miR-92a	-0.07	-0.54; 0.40	0.766	0.900
miR-451	-0.24	-0.66; 0.18	0.261	0.887

Table 24. Association between miRNA levels and SDS scores for the perceived stress domain. Significant associations (p-value<0.05; FDR p-value<0.100) are highlighted in bold.

miRNA	β estimate	95% CI	p-value	FDR p-value
miR-126	0.11	-0.33; 0.54	0.629	0.891
miR-1274B	0.02	-0.48; 0.53	0.924	0.988
miR-142-3p	0.14	-0.38; 0.66	0.589	0.891
miR-191	0.13	-0.28; 0.54	0.537	0.891
miR-19b	0.17	-0.25; 0.58	0.422	0.891
miR-203	0.31	-0.18; 0.81	0.207	0.891
miR-218	0.33	-0.32; 0.98	0.313	0.891
miR-223	0.00	-0.53; 0.54	0.988	0.988
miR-24	0.05	-0.49; 0.60	0.841	0.988
miR-30a-5p	-0.19	-0.79; 0.41	0.530	0.891
miR-30b	0.02	-0.56; 0.59	0.958	0.988
miR-320	0.29	-0.16; 0.75	0.200	0.891
miR-572	0.50	-0.10; 1.09	0.103	0.891
miR-638	0.01	-0.68; 0.70	0.977	0.988
miR-720	0.26	-0.30; 0.83	0.356	0.891
miR-92a	0.24	-0.23; 0.71	0.307	0.891
miR-451	-0.13	-0.57; 0.30	0.545	0.891

Table 25. Association between miRNA levels and SDS scores for the perceived social support domain. Significant associations (p-value<0.05; FDR p-value<0.100) are highlighted in bold.

miRNA	β estimate	95% CI	p-value	FDR p-value
miR-126	2.26	-2.81; 7.33	0.376	0.696
miR-1274B	1.82	-3.44; 7.09	0.491	0.696
miR-142-3p	0.25	-5.23; 5.73	0.927	0.927
miR-191	1.35	-3.53; 6.24	0.580	0.758
miR-19b	2.01	-2.19; 6.20	0.343	0.696
miR-203	0.71	-4.34; 5.77	0.778	0.838
miR-218	-2.30	-8.73; 4.13	0.476	0.696

miR-223	-3.33	-8.87; 2.20	0.232	0.696
miR-24	1.12	-4.27; 6.52	0.679	0.825
miR-30a-5p	5.32	-0.69; 11.33	0.082	0.696
miR-30b	-2.16	-8.13; 3.81	0.470	0.696
miR-320	2.10	-2.70; 6.90	0.384	0.696
miR-572	3.51	-2.96; 9.98	0.282	0.696
miR-638	2.65	-4.44; 9.73	0.458	0.696
miR-720	0.81	-5.19; 6.80	0.789	0.838
miR-92a	2.57	-1.96; 7.10	0.258	0.696
miR-451	2.33	-2.29; 6.96	0.314	0.696

4.2. PART 2

4.2.1. Effect of PM treatment on BEAS-2B cell viability

The effect of the three different types of fine PM (NIST2786, ERM-CZ110, and PM Como) on BEAS-2B cell viability was evaluated by MTT assay and PI staining.

Results from MTT assay (**Figure 14**) show that PM Como exerts a dose-dependent effect, with a viability rate ranging from 0.833 for low-dose to 0.530 for high-dose treatment. Also, ERM-CZ110 displays a dose-dependent effect (viability rate ranging from 0.498 to 0.401), but only for low concentrations of PM. Instead, the effect of NIST2786 is dose-independent for all concentrations tested, also leading to the most severe reduction of cell viability rate (ranging from 0.413 to 0.403). A positive control of cell death was also carried out by treating cells with 10% ethanol, resulting in a viability rate of 0.085.

Figure 14. MTT assay. Viability rate is calculated as the ratio of absorbance for each treatment condition/absorbance of untreated cells.

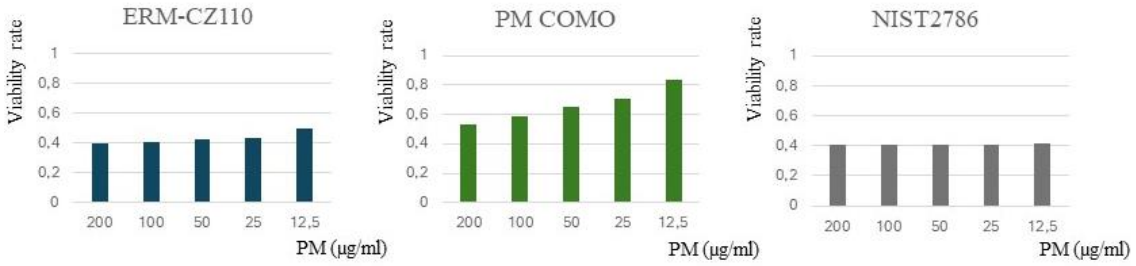

As shown in **Figure 15**, staining with PI also confirms that NIST2786 has the strongest impact on BEAS-2B cell viability, with a percentage of PI+ cells ranging from 26,2% to 1,6%. PM Como and ERCM-CZ100 exert milder effects, with percentages of PI+ cells ranging below 3,2% for all concentrations tested.

Figure 15. PI staining. Panel A: untreated cells, gated for physical parameters (P1); panel B: untreated cells, gated for PI staining (P1/P2); panel C: cells treated with NIST2786, gated for physical parameters (P1); panel D: cells treated with NIST2786, gated for PI staining (P1/P2).

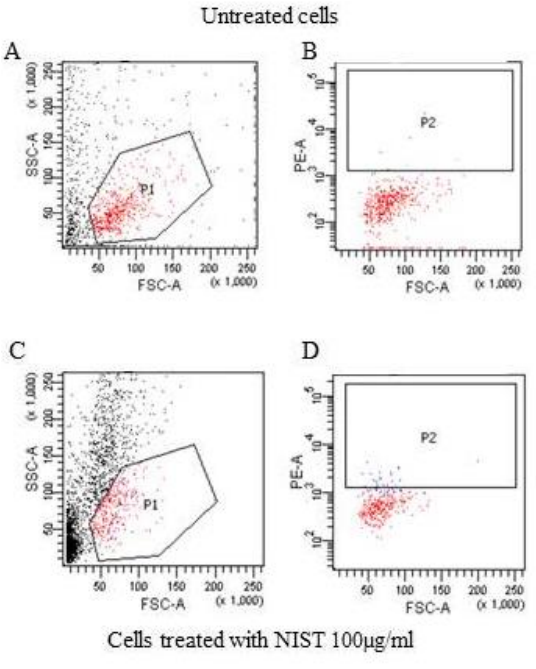

Treatment	Concentration (µg/ml)	%PI+ staining
PM Como	12,5	2,3%
PM Como	25	1,4%
PM Como	50	1,1%
PM Como	100	1,8%
PM Como	200	1,8%
ERM-CZ110	12,5	1,0%
ERM-CZ110	25	1,0%
ERM-CZ110	50	1,4%
ERM-CZ110	100	3,2%
ERM-CZ110	200	1,8%
NIST2786	12,5	1,6%
NIST2786	25	1,7%
NIST2786	50	3,0%
NIST2786	100	6,6%
NIST2786	200	26,2%
Untreated		1,2%
Ethanol 10%		56,8%

Since NIST2786 seems to exert the strongest effect on BEAS-2B cell viability, we chose to focus only on this PM type and to use it at a 100 µg/ml concentration (which corresponds to medium-high exposure [84]) for the next steps of the project. Despite causing a moderate reduction in cell viability, this dose largely preserves the cell morphology, especially if compared to ethanol treatment, as shown in **Figure 16**.

Figure 16. BEAS-2B cells treated with 100 µg/ml NIST2786 (vs untreated or ethanol-treated). Panel A: untreated cells; Panel B: treated cells; Panel C: ethanol-treated. Images were acquired by bright-field microscopy (10X and 20X magnification for left and right panels, respectively; ethanol-treated cells are shown only at 20X).

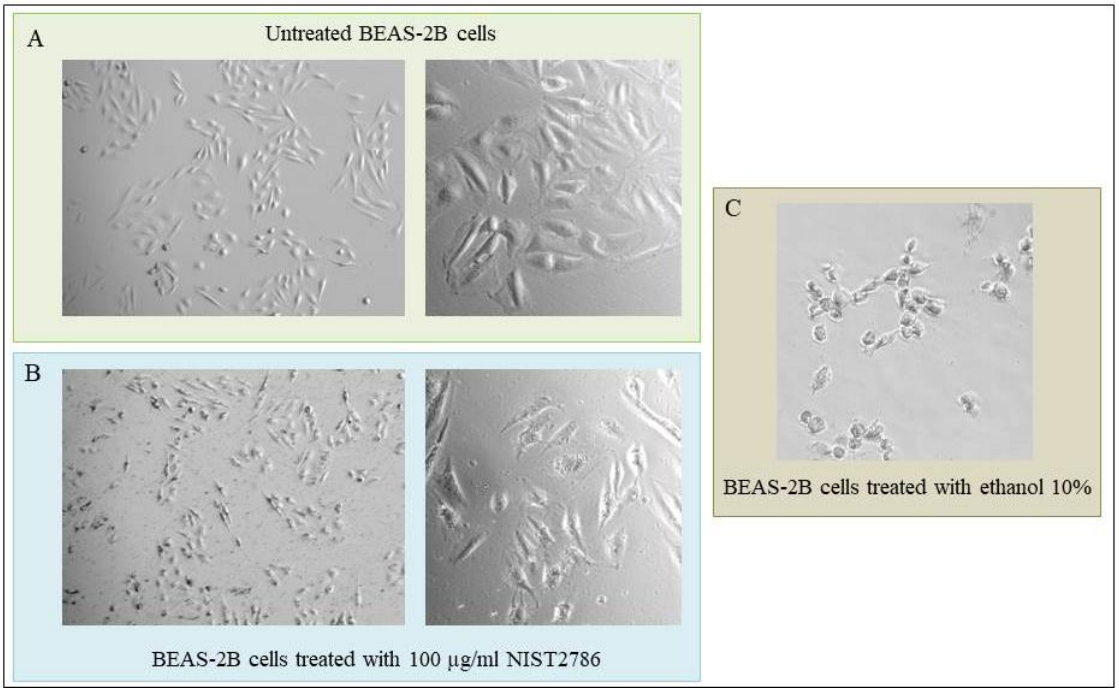

4.2.3. Functional effect of EVs released by BEAS-2B cells on MBMEC BBB model

The effect of BEAS-2B EVs on BBB integrity was assessed by TEER measurement, which was run in quintuplicate for each condition tested (except for MBMECs with no treatment, in quadruplicate). MBMECs were treated with EVs (diluted 1:32) from: 1) EVs collected from untreated BEAS-2B cells after 24h of incubation with medium containing EV-depleted serum ("MBMECs + untreated EVs 24h"); 2) EVs collected after 24h of treatment with 100 µg/ml NIST2786 ("MBMECs + treated EVs 24h); 3) EVs collected after 2h of treatment with 100 µg/ml NIST2786 ("MBMECs + treated EVs 24h); 4) "post-treated" EVs, as defined above ("MBMECs + post-treatment EVs 24h→2h"). Treatment with EVs was carried out from the beginning of the measurement, i.e. right after MBMECs have attached to the transwell inserts and transferred into the cellZscope device.

As shown in **Figure 17**, we observed that all EV treatments tested can affect the TEER of MBMECs, resulting in a reduction of TEER if compared to untreated MBMECs (in red). Of note, the effect of EV treatments starts to become evident from approximately t=70 h of measurement; as time passes, differences become more and more marked, reaching the maximum at the measurement endpoint (t=160 h).

Figure 17. TEER measurement over time. Upper panel: trans-endothelial resistance (TER). Lower panel: capacitance ($_{Ccl}$).

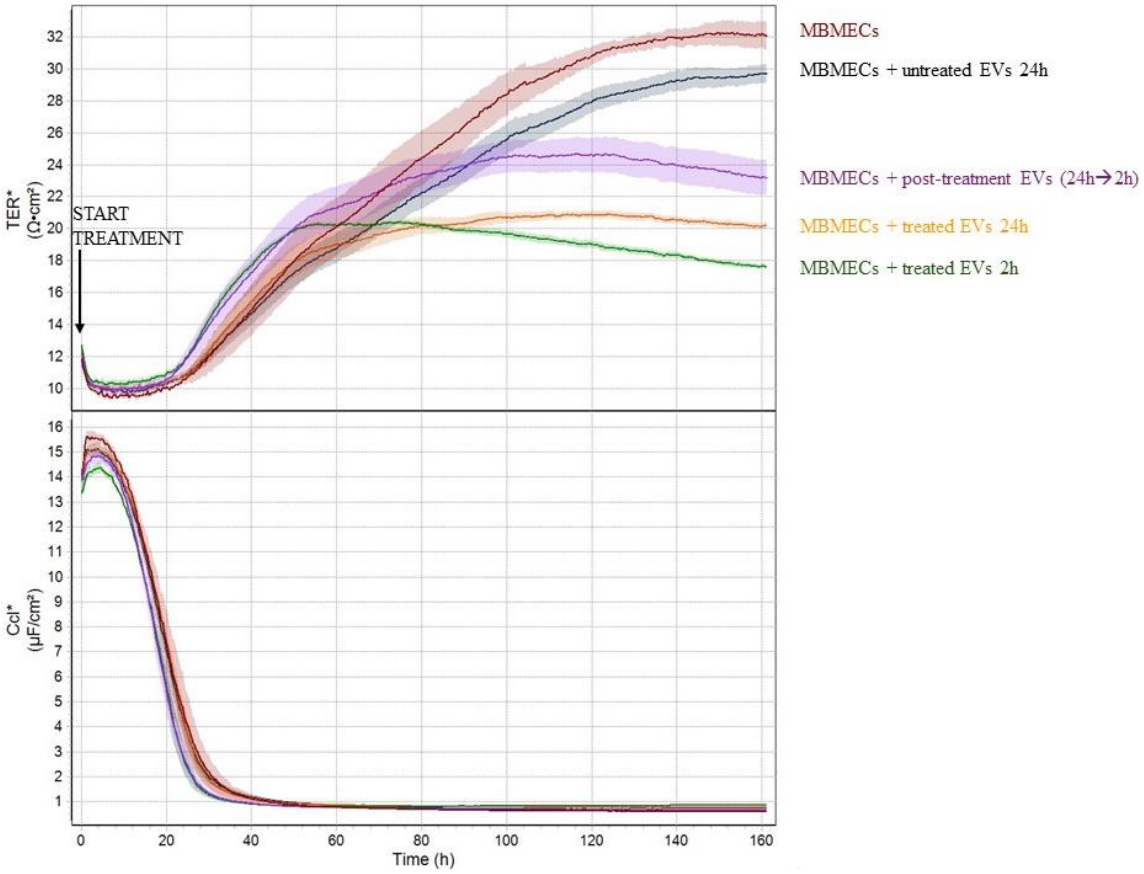

4.2.4. Molecular effect of EVs released by BEAS-2B cells on MBMEC BBB model

The effect of BEAS-2B EVs on blood-brain barrier junctional properties was assessed by gene expression analysis and immunocytochemistry, which were carried out at the endpoint of TEER measurement. As shown in **Figure 18**, treatment with EVs from PM-exposed BEAS-2B cells seems to affect the spatial organization of Claudin 5, a component of tight junction strands, and of VE-cadherin, a glycoprotein localized at adherens juctions. In particular, the junctional pattern of MBMECs + treated EVs 2h is

characterized by presence of numerous ramification-like and disorganized structures, as indicated by orange and white arrows, respectively.

Figure 18. Immunocytochemistry analysis of junctional proteins. Cldn5=Claudin 5; Cdh5=VE-cadherin.

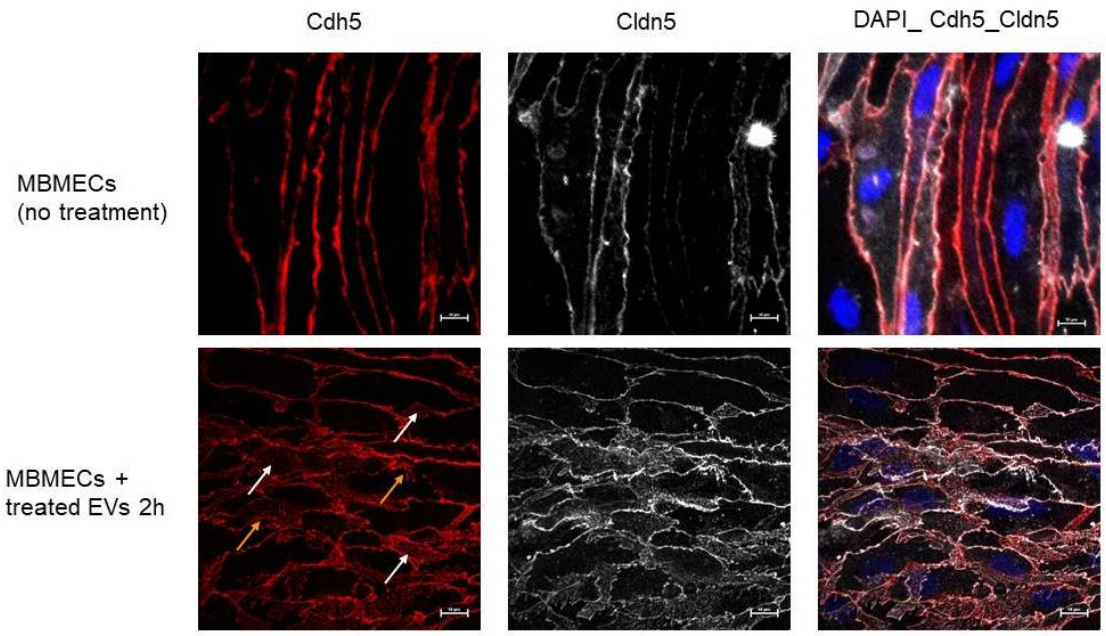

4. DISCUSSION

The first part of this study aimed at investigating the complex interplay between air pollution exposure, the miRNA content of NdEVs, and the severity of MDD.

For this purpose, the first step consisted in exploring the characteristics of NdEVs, which were enriched starting from total plasma EVs by immunoaffinity capture, an isolation technique which relies on the formation of an immunocomplex between the neuron-enriched L1CAM adhesion molecule and an antibody targeting the ectodomain of this protein [85,86]. The efficiency of this protocol was proved to be overall high, with more than 90% of events corresponding to L1CAM+ EVs in the NdEV-enriched fraction. However, considering that the detection threshold of the flow cytometer is >200 nm and that the expected size of EVs can be lower than 100 nm, it is not possible to determine whether the smaller fraction of EVs is captured with the same efficiency as larger EVs with this methodology.

Instead, NTA allows the detection of particles spanning from 0 to 1000 nm, thus including also smaller particles and being more suitable for EV quantification. Based on NTA, immunocaptured EVs were on average smaller than total EVs (182±9 nm vs 218±12 nm). Although it is not clear whether and how different cell types release EVs with different sizes *in vivo* (mainly due to the difficulty of separating EV subtypes from complex biological matrices), it is possible that neurons preferentially release exosomes than microvesicles, therefore resulting in an EV pool with lower average dimensions. Although our findings are hampered by the reduced number of EV samples analyzed, they are in accordance with what observed by Saeedi and colleagues, who similarly reported that NdEVs have a smaller diameter than total EVs; intriguingly, they also observed that NdEVs were even smaller in subjects with MDD (n=40) if compared to healthy controls (n=20), suggesting that NdEV size might be also related to pathophysiological states [87].

Also, according to NTA data, the NdEV fraction corresponded to approximately 4.5% of total EVs. This percentage is generally in line to that measured by NTA by Mustapic and co-workers (9.6%), considering that total EVs were obtained by a precipitation method with higher yield than ultracentrifugation [67]; instead, as said before, it is

difficult to compare these values with others obtained with other methodologies than NTA due to instrument sensitivity bias. Besides, the number of plasma EVs and the proportion of each EV subtype are highly variable due to a multitude of factors – most of which remain unknown – not only under pathological conditions, but also in apparently healthy individuals [88]. Also, the choice of the marker for the isolation of specific EV subpopulations might influence the percentage and size of detected EVs; indeed, a study showed that leveraging ATPase Na+/K+ transporting subunit alpha 3 (ATP1A3) as a neuron-specific epitope resulted in higher percentage of NdEVs if compared to L1CAM-based methods [89].

L1CAM-based immunoaffinity capture was proposed for the first time by two independent reports around ten years ago [85,86]. Since then, some criticism has been raised around this method, mainly due to the dubious specificity of L1CAM and the presence of soluble forms of this protein in plasma [90]. As a matter of fact, L1CAM is also expressed (to a lesser extent) in non-neuronal cells such as oligodendrocytes, melanocytes, and some types of immune cells, and its extracellular domain can be cleaved by multiple proteases [91]. Nevertheless, over time, multiple studies exploiting this protocol have highlighted the potentiality of L1CAM+ blood NdEVs as a source of biomarkers for multiple neurological and psychiatric disorders, including Alzheimer's disease [92], Parkinson's disease [93], multiple sclerosis [94], amyotrophic lateral sclerosis [95], schizophrenia [96], and MDD [87,97,98]. Such findings support that L1CAM+ blood NdEVs provide a unique window on brain-related processes if compared to other circulating biomarkers, whose origin cannot be traced back to specific tissues. In particular, a recent report showed that L1CAM-based immunocapture of NdEVs generates reproducible miRNA fingerprints, possibly paving the way for translational applications in clinical practice [99].

In this study, 54 miRNAs were selected for the analysis of the study population. The choice was based on a preliminary miRNA profiling step, which was carried out on total EV and NdEV pools from healthy subjects and MDD cases, as well as on literature/database search of brain-specific miRNAs. The limited number of miRNA species identified within NdEVs (52 out of 754 miRNAs screened) is consistent with what expected for a well-defined EV subpopulation, as miRNA expression patterns are cell- / tissue-specific [81], and most EVs contain a low copy number of miRNAs [100]. Overall, the selected miRNA panel was

predicted to target 128 genes, which are mainly implied in intracellular signaling, cell response to stress/external stimuli, immune system regulation, and cell senescence. Among the top-10 genes regulated by NdEV miRNAs, *SLC7A11* encodes a cystine/glutamate antiporter with antioxidant functions, which has been implied in multiple neuroinflammation-based central nervous system (CNS) diseases; of note, this gene is highly expressed in astrocytes and its expression levels are strongly modulated by external stressors [101]. Also, *TP53* and *FYCO1* are implied in stress response and regulation of senescence/apoptosis by participating in DNA repair and autophagy, respectively [102,103]. Similarly, other highly enriched genes are implied in cell adaptation to external stimuli (e.g. *ARPP19*, a cell cycle regulator [104], and *DNMT1*, implied in epigenetic remodeling [105]) and neuroinflammation (e.g. *TNFRSF10B*, encoding a Tumor Necrosis Factor receptor [106]). Nevertheless, further mechanistic studies are needed to elucidate the regulatory role of these NdEV-borne miRNAs in recipient cells.

The two-phase approach employed in this study for miRNA analysis has advantages and limitations. On one side, it allowed to restrict the analysis on the study population to a small number of miRNA species, which were subsequently quantified more precisely in triplicate. On the other side, miRNAs which are highly expressed only in a low percentage of subjects might have been screened out; indeed, the 52 miRNAs were selected by analyzing EV pools derived from multiple subjects, resulting in flattened inter-individual variability of miRNA expression and loss of "outliers". For this reason, brain-specific miRNAs like miR-9-5p and miR-124-3p were screened out and excluded from the original miRNA panel as both were not detected in any of the 6 NdEV pools; nevertheless, they were detected in a small fractions of the participants, where they might play a relevant role in depression pathogenesis. In this context, two previous studies have evaluated the miRNA cargo of plasma NdEVs in subjects with MDD. Saeedi and colleagues identified a three-NdEV miRNA signature (miR-21-5p, miR-30d-5p, and miR-486-5p) that was associated with antidepressant treatment response [87]; while Burrows and co-workers showed that subjects with MDD had lower NdEV miR-93 expression than healthy controls, and that lower miR-93 was associated with increased serum concentrations of leptin and pro-inflammatory markers [98]. Nevertheless, to the best of my knowledge, no study has ever evaluated the association of air pollution (or other inhaled toxicants) with the molecular cargo of NdEVs, and whether such content can be associated with MDD severity.

This study was conducted on a population of 93 subject with MDD, whose demographic and clinical characteristics were generally in line with those of the larger DeprAir study population and with other populations of subjects with MDD, as described in literature; indeed, as expected, the majority of subjects were females, and about one third had a family history of MDD [58,107,108]. In this population, we observed a positive association between NO_2 exposure on the day before blood drawing (day -1) and 4 miRNAs, namely miR-1274B, miR-320, miR-720, and miR-451. Instead, exposures to both NO_2 and $PM_{2.5}$ at lag 0-180 were positively associated with miR-19b. Besides, multiple NdEV miRNAs were found to be associated with MDD severity scales; specifically, 4 miRNAs (miR-126, miR-19b, miR-572, and miR-638) were negatively associated with the MADRS score, 2 miRNAs (miR-218 and miR-572) were negatively associated with the HAM-D score, 8 miRNAs (miR-126, miR-142-3p, miR-19b, miR-24, miR-30a-5p, miR-30b, miR-638, and miR-451), were associated with better functioning, as indicated by higher CGI scores, 8 miRNAs (miR-126, miR-142-3p, miR-19b, miR-218, miR-30b, miR-572, miR-638, and miR-451) were negatively associated with CGI scores, and 2 miRNAs were negatively associated with the SDS scale (miR-126 with the disability and relationship domains; and miR-638 with the disability domain).

NO_2 is a traffic-derived gaseous pollutant that can easily cross the epithelial barrier in the airways; once in an aqueous environment, it can spontaneously decompose to form nitric acid (HNO_3) and nitric oxide (NO). NO is a well-known pleiotropic signaling molecule which is implied in a plethora of biological processes such as vasodilation, neurotransmission, and inflammation [109]; of note, high levels of NO can increase the permeability of the BBB, resulting in the uncontrolled, potentially deleterious passage of molecules across the blood-brain interface [110]. Therefore, it is possible that inhaled NO_2 might modulate the molecular content of EVs released by the brain, and that such changes might occur rapidly due to the direct action of this pollutant. Indeed, all the miRNAs associated with NO_2 exposure have been previously found within EVs [111–114], and circulating miR-451 has been previously found to be positively associated with NO_2 exposure [115]; however, the authors did not investigate whether such miRNA was encapsulated within EVs or not. Of note, increased miR-451 levels were associated with reduced MDD severity (higher GAF and lower CGI scores). MiR-451 is an anti-inflammatory miRNA which is involved in the pathogenesis of several neurological and

psychiatric disorders [116–118]. A previous report has shown that MDD subjects have lower circulating miR-451 if compared to healthy controls, and that anti-depressant treatment increased its expression levels [119]. Also, serum levels of miR-451 were found to negatively correlate with MDD severity, both in humans and in murine models; indeed, such miRNA has been proposed as a potential target for MDD therapy as inducing its overexpression in the prefrontal cortex reversed dendrite plasticity and ameliorated MDD symptoms in mice [120].

Differently from NO_2, $PM_{2.5}$ is well-known to regulate EV release and ncRNA content, with either adaptive or detrimental effects on recipient cells [121,122]. However, this is the first research report analyzing its association with NdEVs. Due to the presence of the BBB, fine PM mainly exerts its noxious effect on the brain via the indirect pathway; therefore, the impact on NdEV miRNAs might be more limited, especially in the short term. Indeed, only one miRNA, i.e. miR-19b, was found to be positively associated with chronic $PM_{2.5}$ exposure in the 6-month window preceding blood drawing, while no associations were found at days 0 and -1. Interestingly, a previous study has found a positive association between $PM_{2.5}$ exposure in the same time lag and miR-19b carried by serum EVs [123]. Of note, increased miR-19b levels were also associated with NO_2 increments in the same time lag, suggesting that it might be responsive to multiple chronic stressors. Besides, this miRNA was negatively associated with MDD severity according to the MADRS, GAF, and CGI scales. MiR-19b is a widely expressed oncogenic miRNAs which regulates a plethora of biological processes, including cell proliferation, migration and apoptosis; indeed, alterations in the expression levels of this miRNA have been detected in multiple oncologic, cardiovascular and neurodegenerative diseases [124]. In the brain, miR-19b is a crucial regulator of neural stem cell differentiation into mature neurons; of note, early-life stress leads to the downregulation of this miRNA, resulting in increased risk of mental diseases later in life [125]..

The potentially beneficial role - at least in the brain - of NdEVs and their miRNA cargo is also supported by our observation that increments of NdEV miRNAs are negatively associated with all severity scales considered (both scales that are specific for MDD, i.e. the MADRS and HAM-D scales, and those related to general functioning, i.e. GAF, CGI and SDS scales). Accordingly, the transfer of NdEV miRNAs to recipient cells have been previously speculated to serve as a targeted attempt to counter

neurodegeneration and inflammation in the CNS [126]. Supporting this hypothesis, among the 10 miRNAs associated with MDD severity, the stress-responsive, neuroprotective miR-218 [127,128] has been previously associated with decreased HAMD scores [129] and has been detected within NdEVs, which in turn promoted excitatory synapse formation in hippocampal neurons [130]. Also miR-126 and miR-572, which are associated with 5 and 3 severity scales in this study, respectively, have been found to be downregulated in MDD patients and their expression levels are restored by pharmacological and electroconvulsive therapies [131,132].

Despite being innovative and having several strengths, the present study has also some limitations. First, it is a cross-sectional study, so it is not possible to analyze longitudinal time trends or establish cause-and-effect relationships. Second, the estimation of air pollution exposure does not take into account potentially confounding factors such as the time spent at the residential address, commuting habits, as well as indoor air quality. Third, it does not investigate whether the identified differences in miRNA cargo that are associated with air pollution or with MDD severity have a functional impact on recipient cells. Future studies on cellular or animal models are needed to elucidate the biological significance of such miRNA alterations.

Instead, studying the effect of air pollution-induced EVs on the brain was the main focus of the second part of this study, which aimed at investigating the effect of EVs released by PM-treated bronchial cells on an *in vitro* model of BBB.
First, we evaluated the effect of three different types of fine PM, i.e. ERM-CZ110, NIST2786, and urban $PM_{2.5}$ collected in Como, on the viability of BEAS-2B bronchial epithelial cells. Cell viability was assessed via two different assays, which provide complementary information on the "health status" of cells. The MTT assay is a colorimetric test that measures mitochondrial activity (as the reduction of MTT into purple formazan crystals is mainly catalyzed by mitochondrial dehydrogenases); instead, PI is a membrane-impermeant nucleic acid intercalator that enters and stains cells with compromised membrane integrity, i.e. late apoptotic and necrotic cells [133].

Based on MTT assay, urban PM from Como and ERM-CZ110 caused a dose-dependent reduction of cell viability, which was more marked for ERM-CZ110-treated cells at all doses considered; instead, NIST2786 exerted the strongest effect at the concentrations

tested in a seemingly dose-independent manner. On the contrary, when considering PI staining, PM from Como and ERM-CZ110 caused only a minor reduction in cell viability at all doses tested (if compared to what observed for untreated cells), while NIST2786 had a dose-dependent effect, with the highest concentration (200 μg/ml) causing a significant increment in cell death rate.

This brings us to some considerations regarding the origin, the biochemical composition and the impact of PM on the viability and metabolism of treated cells. The mildest effect of PM from Como might be explained considering that it derives from airborne particles collected in an outdoor urban environment, which have a more diverse composition than traffic-related PM (i.e. ERM-CZ110) or indoor PM (i.e. NIST2786). Of note, NIST2786 is highly enriched in heavy metals if compared to PM from Como (approximately ten-fold enrichment of chromium, and five-fold of cadmium, manganese and copper), which are well-known to be toxic for airway cells by causing oxidative stress, genomic instability, and mitochondrial dysfunction [134,135]. This might – at least partially - explain the discrepancy of the results obtained for NIST2786 by MTT assay and PI staining: NIST2786 might impair mitochondrial homeostasis, without causing necrosis or late-stage cell death in the short term. Accordingly, a previous study found that NIST2786-induced reduction of BEAS-2B cell viability can be countered by eupatilin, an anti-oxidative compound targeting ROS production (which mainly occurs in mitochondria) [136].

In the end, the choice of focusing on 100 μg/ml NIST2786 was made in the view of providing treated cells with a strong stimulus (corresponding to medium-high, yet biologically relevant PM exposure [137]), bearing a late-apoptosis/necrosis rate that we considered as acceptable (<10%), also considering that the cell morphology was largely preserved following PM treatment. Nevertheless, we acknowledge this as a potential limitation of our study, as additional experiments are needed to comprehensively evaluate the impact of different PM types and doses on BEAS-2B cells; in addition, NIST2786 might not be fully representative of actual real-world exposure scenarios, considering its chemical characteristics and time of collection. Next, MBMECs were treated with EVs derived from BEAS-2B cells in order to assess whether they might mediate the toxic effect of PM on the BBB. Here, we observed that EVs derived from PM-treated cells caused a reduction in TEER of MBMECs, suggesting a functional

impairment of our BBB model. Indeed, TEER is a measure of paracellular resistance (i.e. resistance to the passage of electric current or substances through the intercellular spaces), which is governed by cell-cell junctions in a BBB endothelial monolayer. However, such impairment was not paralleled by cell death, as cell membrane capacitance (C_{cl}), which is an index of transcellular resistance (i.e. resistance to the passage of electric current or substances through cells by endocytosis, diffusion, or active transport) remained low. On the molecular side, we also observed that EVs derived from PM-treated cells alter the spatial organization of tight junction proteins, forming more relaxed, net-like structures; nevertheless, additional experiments are needed to confirm whether such structural changes might be responsible for the observed loss of BBB integrity.

Despite being preliminary, our findings open to novel, exciting perspectives on the mechanisms mediating the toxicity of fine PM on the brain. Indeed, to the best of my knowledge, this is the first study evaluating the functional impact of PM-induced EVs on a BBB model. Previous studies have shown that BEAS-2B cells treated with $PM_{2.5}$ release EVs that increase the permeability of recipient endothelial cells; indeed, such EVs were enriched with circular RNAs that were predicted to target tight and adherens junctions [138]. Besides, there is evidence that PM itself can impair cell-cell junctions of endothelial monolayers, thus favoring the transmigration of immune cells to the brain; and that PM-induced EVs might participate in mediating neurotoxicity through their protein cargo [139]. Nevertheless, as discussed before, it is probable that only the ultrafine fraction of PM can reach the BBB and exert directly its noxious action. Also, EVs derived from the blood of subjects exposed to high PM levels stimulate endothelial activation, if compared to EVs from low-exposed subjects [140]. This might be in accordance with our findings, supporting that EVs released from peripheral tissues following high PM exposure might promote endothelial dysfunction.

We acknowledge that this study has some limitations, which include: 1) starting the treatment of MBMECs with EVs right after seeding the cells on the inserts, when the BBB is still not formed. These data should be integrated with an experiment evaluating the effect of treatment when the BBB is already formed (when the TEER graph reaches the plateau), which is more representative of the BBB in the adult brain; 2) possible contamination of EV preparations with PM residues. Although there is some evidence

suggesting that EVs might interact with and transport ultrafine PM through the organisms [141], it would be desirable to obtain EV preparations without residual PM traces, as they might themselves compromise BBB properties. However, even in the "post-treat" condition, which was added to minimize PM carryovers, it is not possible to completely avoid such contamination under our experimental settings. A possible strategy might involve fixing BEAS-2B cells, treating them with PM, and then following the protocol for EV collection: in this case, the potential effect on BBB would be mediated only by the PM fraction isolated with this methodology, as the supernatant would be depleted of EVs; 3) lack of evaluation of the EV cargo, in order to determine if the effect on MBMECs is mediated by specific molecules. Further experiments are needed to gain deeper insights into the molecular mechanisms of PM-induced, EV-mediated BBB dysfunction.

5. CONCLUSIONS AND FUTURE PERSPECTIVES

In the first part of the study, plasma NdEVs were found to retain unique characteristics if compared to total EVs, regarding both their size and miRNA content. Besides, NdEV-enriched miRNAs were predicted to target genes implied in the response to stress and external cues, as well as in the modulation of immune-related and signaling pathways, suggesting that they might be important players at the interface between air pollution exposure and brain pathophysiology. Indeed, exposure to fine PM and NO_2 was found to be associated with alterations in the miRNA content of plasma NdEVs, with two of the miRNAs upregulated by air pollution (miR-451 and miR-19b) being also negatively associated with MDD severity. These findings suggest for the first time that environmentally induced changes in NdEV miRNAs might be a novel adaptive mechanism to counter the detrimental effects of inhaled toxicants on the brain. Also, the identification of NdEV miRNAs associated with MDD severity might pave the way for novel, non-invasive strategy for MDD prognosis, which would be of extreme relevance considering the lack of lab methods for MDD evaluation. Given the huge potentiality of NdEVs at the nexus of external environment and psychiatric disorders, this topic will be more extensively investigated as part of the FREEDOM project (Further Exploring Environmental Determinants of Mental health, PRIN 2022). Here, the analysis of NdEV miRNAs will be extended to a larger sample of the DeprAir study population (n=200 subjects), thus strengthening the statistical power and generalizability of the findings, which are critical for the identification of robust biomarkers. In addition, the FREEDOM study will involve the quantification of NdEV size and count in the study participants, which might be also modulated by disease severity or environmental cues. In this context, greenness exposure (i.e., exposure to green spaces) will also be evaluated as an additional external factor potentially modulating NdEV characteristics and MDD prognosis.

Overall, the results reported in the first part of this thesis highlight the importance of peripheral EVs released from the CNS in the air pollution-MDD interplay. However, also EVs derived from peripheral tissues can affect the CNS, as observed in the second part of the study. Here, PM treatment of airway cells was found to induce the release of EVs, which in turn compromised the permeability and the pattern of junctional proteins

of the BBB. As the BBB is known to be disrupted in MDD and other pathological states, these findings might therefore suggest a novel, EV-mediated pathway linking air pollution exposure to CNS damage. Further *in vivo* studies are warranted to better elucidate this unexplored mechanism.

In conclusion, the work of this thesis contributes to expanding the current knowledge on the role of EVs in the complex relationship between air pollution exposure and MDD, with implications for research and clinical applications.

6. REFERENCES

1. World Health Organization. Ambient (outdoor) air pollution. https://www.who.int/news-room/fact-sheets/detail/ambient-(outdoor)-air-quality-and-health (2021).

2. Kim, K.-H., Kabir, E. & Kabir, S. A review on the human health impact of airborne particulate matter. *Environ. Int.* **74**, 136–143 (2015).

3. Zhou, X., Zhou, X., Wang, C. & Zhou, H. Environmental and human health impacts of volatile organic compounds: A perspective review. *Chemosphere* **313**, 137489 (2023).

4. Kampa, M. & Castanas, E. Human health effects of air pollution. *Environ. Pollut.* **151**, 362–367 (2008).

5. GBD 2021 Risk Factors Collaborators. Global burden and strength of evidence for 88 risk factors in 204 countries and 811 subnational locations, 1990-2021: a systematic analysis for the Global Burden of Disease Study 2021. *Lancet Lond. Engl.* **403**, 2162–2203 (2024).

6. Pryor, J. T., Cowley, L. O. & Simonds, S. E. The Physiological Effects of Air Pollution: Particulate Matter, Physiology and Disease. *Front. Public Health* **10**, (2022).

7. Uher, R., Payne, J. L., Pavlova, B. & Perlis, R. H. Major depressive disorder in DSM-5: implications for clinical practice and research of changes from DSM-IV. *Depress. Anxiety* **31**, 459–471 (2014).

8. World Health Organization. Depression. https://www.who.int/news-room/fact-sheets/detail/depression (2021).

9. Friedrich, M. J. Depression Is the Leading Cause of Disability Around the World. *JAMA* **317**, 1517 (2017).

10. Briley, M. & Lépine. The increasing burden of depression. *Neuropsychiatr. Dis. Treat.* 3 (2011) doi:10.2147/NDT.S19617.

11. ISTAT. Mental health at various stages of life. https://www.istat.it/en/archivio/219812 (2018).

12. Taliaz, D. *et al.* Optimizing prediction of response to antidepressant medications using machine learning and integrated genetic, clinical, and demographic data. *Transl. Psychiatry* **11**, 1–9 (2021).

13. Dean, J. & Keshavan, M. The neurobiology of depression: An integrated view. *Asian J. Psychiatry* **27**, 101–111 (2017).

14. Saveanu, R. V. & Nemeroff, C. B. Etiology of Depression: Genetic and Environmental Factors. *Psychiatr. Clin.* **35**, 51–71 (2012).

15. Klengel, T. & Binder, E. B. Gene—Environment Interactions in Major Depressive Disorder. *Can. J. Psychiatry* **58**, 76–83 (2013).

16. Flint, J. The genetic basis of major depressive disorder. *Mol. Psychiatry* **28**, 2254–2265 (2023).

17. Howard, D. M. *et al.* Genome-wide meta-analysis of depression identifies 102 independent variants and highlights the importance of the prefrontal brain regions. *Nat. Neurosci.* **22**, 343–352 (2019).

18. Borroni, E., Pesatori, A. C., Bollati, V., Buoli, M. & Carugno, M. Air pollution exposure and depression: A comprehensive updated systematic review and meta-analysis. *Environ. Pollut. Barking Essex 1987* **292**, (2022).

19. Yang, T., Wang, J., Huang, J., Kelly, F. J. & Li, G. Long-term Exposure to Multiple Ambient Air Pollutants and Association With Incident Depression and Anxiety. *JAMA Psychiatry* **80**, 305–313 (2023).

20. Li, N. *et al.* Exposure to indoor air pollution from solid fuel and its effect on depression: a systematic review and meta-analysis. *Environ. Sci. Pollut. Res. Int.* **29**, 49553–49567 (2022).

21. Oberdörster, G. *et al.* Translocation of Inhaled Ultrafine Particles to the Brain. *Inhal. Toxicol.* **16**, 437–445 (2004).

22. Hahad, O. *et al.* Ambient Air Pollution Increases the Risk of Cerebrovascular and Neuropsychiatric Disorders through Induction of Inflammation and Oxidative Stress. *Int. J. Mol. Sci.* **21**, 1–24 (2020).

23. Gładka, A., Rymaszewska, J. & Zatoński, T. Impact of air pollution on depression and suicide. *Int. J. Occup. Med. Environ. Health* **31**, 711–721 (2018).

24. Wu, S., Yin, Y. & Du, L. Blood-Brain Barrier Dysfunction in the Pathogenesis of Major Depressive Disorder. *Cell. Mol. Neurobiol.* **42**, 2571–2591 (2022).

25. Boda, E., Rigamonti, A. E. & Bollati, V. Understanding the effects of air pollution on neurogenesis and gliogenesis in the growing and adult brain. *Curr. Opin. Pharmacol.* **50**, 61–66 (2020).

26. Gavito-Covarrubias, D. *et al.* Epigenetic mechanisms of particulate matter exposure: air pollution and hazards on human health. *Front. Genet.* **14**, (2024).

27. Yuan, H., Mischoulon, D., Fava, M. & Otto, M. W. Circulating microRNAs as biomarkers for depression: Many candidates, few finalists. *J. Affect. Disord.* **233**, 68–78 (2018).

28. Żurawek, D. & Turecki, G. The miRNome of Depression. *Int. J. Mol. Sci.* **22**, 11312 (2021).

29. Van Niel, G., D'Angelo, G. & Raposo, G. Shedding light on the cell biology of extracellular vesicles. *Nat. Rev. Mol. Cell Biol.* **19**, 213–228 (2018).

30. Matsumoto, J., Stewart, T., Banks, W. A. & Zhang, J. The Transport Mechanism of Extracellular Vesicles at the Blood-Brain Barrier. *Curr. Pharm. Des.* **23**, 6206–6214 (2018).

31. Doyle, L. & Wang, M. Overview of Extracellular Vesicles, Their Origin, Composition, Purpose, and Methods for Exosome Isolation and Analysis. *Cells* **8**, 727 (2019).

32. Zhang, Y., Liu, Y., Liu, H. & Tang, W. H. Exosomes: Biogenesis, biologic function and clinical potential. *Cell Biosci.* **9**, 1–18 (2019).

33. Tetta, C., Ghigo, E., Silengo, L., Deregibus, M. C. & Camussi, G. Extracellular vesicles as an emerging mechanism of cell-to-cell communication. *Endocrine* **44**, 11–19 (2013).

34. Koga, Y. *et al.* Exosome can prevent RNase from degrading microRNA in feces. *J. Gastrointest. Oncol.* **2**, 215–222 (2011).

35. Mulcahy, L. A., Pink, R. C. & Carter, D. R. F. Routes and mechanisms of extracellular vesicle uptake. *J. Extracell. Vesicles* **3**, (2014).

36. Yáñez-Mó, M. *et al.* Biological properties of extracellular vesicles and their physiological functions. *J. Extracell. Vesicles* **4**, 1–60 (2015).

37. Nowak, M., Górczyńska, J., Kołodzińska, K., Rubin, J. & Choromańska, A. Extracellular Vesicles as Drug Transporters. *Int. J. Mol. Sci.* **24**, 10267 (2023).

38. Ciferri, M. C., Quarto, R. & Tasso, R. Extracellular Vesicles as Biomarkers and Therapeutic Tools: From Pre-Clinical to Clinical Applications. *Biology* **10**, 359 (2021).

39. Monti, P., Solazzo, G., Ferrari, L. & Bollati, V. Extracellular Vesicles: Footprints of environmental exposures in the aging process? *Curr. Environ. Health Rep.* (2021) doi:10.1007/S40572-021-00327-3.

40. Shetty, A. K. & Upadhya, R. Extracellular Vesicles in Health and Disease. *Aging Dis.* **12**, 1358–1362 (2021).

41. Cuomo-Haymour, N. *et al.* Differential expression of serum extracellular vesicle microRNAs and analysis of target-gene pathways in major depressive disorder. *Biomark. Neuropsychiatry* **6**, 100049 (2022).

42. Wei, Z. X. *et al.* Exosomes from patients with major depression cause depressive-like behaviors in mice with involvement of miR-139-5p-regulated neurogenesis. *Neuropsychopharmacol. Off. Publ. Am. Coll. Neuropsychopharmacol.* **45**, 1050–1058 (2020).

43. Eckhardt, C. M., Baccarelli, A. A. & Wu, H. Environmental Exposures and Extracellular Vesicles: Indicators of Systemic Effects and Human Disease. *Curr. Environ. Health Rep.* **9**, 465–476 (2022).

44. Mobarrez, F., Antoniewicz, L., Hedman, L., Bosson, J. A. & Lundbäck, M. Electronic cigarettes containing nicotine increase endothelial and platelet derived extracellular vesicles in healthy volunteers. *Atherosclerosis* **301**, 93–100 (2020).

45. Nancy, R.-T. & Dirk P, D. Viral effects on the content and function of extracellular vesicles. *Nat. Rev. Microbiol.* **15**, (2017).

46. Banks, W. A. *et al.* Transport of Extracellular Vesicles across the Blood-Brain Barrier: Brain Pharmacokinetics and Effects of Inflammation. *Int. J. Mol. Sci.* **21**, 4407 (2020).

47. Ramos-Zaldívar, H. M. *et al.* Extracellular vesicles through the blood–brain barrier: a review. *Fluids Barriers CNS* **19**, 60 (2022).

48. Kadry, H., Noorani, B. & Cucullo, L. A blood–brain barrier overview on structure, function, impairment, and biomarkers of integrity. *Fluids Barriers CNS* **17**, 69 (2020).

49. Abdelsalam, M., Ahmed, M., Osaid, Z., Hamoudi, R. & Harati, R. Insights into Exosome Transport through the Blood–Brain Barrier and the Potential Therapeutical Applications in Brain Diseases. *Pharmaceuticals* **16**, 571 (2023).

50. Shahjin, F., Chand, S. & Yelamanchili, S. V. Extracellular Vesicles as Drug Delivery Vehicles to the Central Nervous System. *J. Neuroimmune Pharmacol.* **15**, 443–458 (2020).

51. Ruan, J., Miao, X., Schlüter, D., Lin, L. & Wang, X. Extracellular vesicles in neuroinflammation: Pathogenesis, diagnosis, and therapy. *Mol. Ther.* **29**, 1946–1957 (2021).

52. Markaki, I. *et al.* Isolation of L1CAM-Extracellular Vesicles Reveals Signs of Insulin Resistance in Parkinson's Disease. *Mov. Disord. Off. J. Mov. Disord. Soc.* **38**, 2136–2137 (2023).

53. Krokidis, M. G. *et al.* Lipidomic Analysis of Plasma Extracellular Vesicles Derived from Alzheimer's Disease Patients. *Cells* **13**, 702 (2024).

54. Qin, Y. *et al.* Whole-Transcriptome Analysis of Serum L1CAM-Captured Extracellular Vesicles Reveals Neural and Glycosylation Changes in Autism Spectrum Disorder. *J. Mol. Neurosci. MN* **72**, 1274–1292 (2022).

55. A, K. *et al.* Small extracellular vesicles in plasma reveal molecular effects of modified Mediterranean-ketogenic diet in participants with mild cognitive impairment. *Brain Commun.* **4**, (2022).

56. Eitan, E. *et al.* In a randomized trial in prostate cancer patients, dietary protein restriction modifies markers of leptin and insulin signaling in plasma extracellular vesicles. *Aging Cell* **16**, 1430–1433 (2017).

57. Suire, C. N. *et al.* Walking speed decline in older adults is associated with elevated pro-BDNF in plasma extracellular vesicles. *Exp. Gerontol.* **98**, 209–216 (2017).

58. Borroni, E. *et al.* Understanding the Interplay between Air Pollution, Biological Variables, and Major Depressive Disorder: Rationale and Study Protocol of the DeprAir Study. *Int. J. Environ. Res. Public. Health* **20**, 5196 (2023).

59. Quilty, L. C. *et al.* The structure of the Montgomery–Åsberg depression rating scale over the course of treatment for depression. *Int. J. Methods Psychiatr. Res.* **22**, 175–184 (2013).

60. Sharp, R. The Hamilton Rating Scale for Depression. *Occup. Med.* **65**, 340 (2015).

61. Busner, J. & Targum, S. D. The Clinical Global Impressions Scale. *Psychiatry Edgmont* **4**, 28–37 (2007).

62. Sheehan, K. H. & Sheehan, D. V. Assessing treatment effects in clinical trials with the Discan metric of the Sheehan Disability Scale. *Int. Clin. Psychopharmacol.* **23**, 70 (2008).

63. Aas, I. M. Guidelines for rating Global Assessment of Functioning (GAF). *Ann. Gen. Psychiatry* **10**, 2 (2011).

64. Silibello, C. *et al.* Modelling of PM10 concentrations over Milano urban area using two aerosol modules. *Environ. Model. Softw.* **23**, 333–343 (2008).

65. Yi, W. *et al.* Examining the association between apparent temperature and admissions for schizophrenia in Hefei, China, 2005-2014: A time-series analysis. *Sci. Total Environ.* **672**, 1–6 (2019).

66. Pergoli, L. *et al.* Extracellular vesicle-packaged miRNA release after short-term exposure to particulate matter is associated with increased coagulation. *Part. Fibre Toxicol.* **14**, 32 (2017).

67. Mustapic, M. *et al.* Plasma Extracellular Vesicles Enriched for Neuronal Origin: A Potential Window into Brain Pathologic Processes. *Front. Neurosci.* **11**, 278 (2017).

68. Cantone, L., Hoxha, M. & Bollati, V. Characterization of microvesicles using the MACSQuant® Analyzer. https://bit.ly/3w323tG.

69. Ferrari, L. *et al.* Extracellular Vesicles Released by Colorectal Cancer Cell Lines Modulate Innate Immune Response in Zebrafish Model: The Possible Role of Human Endogenous Retroviruses. *Int. J. Mol. Sci.* **20**, 3669 (2019).

70. Andersen, C. L., Jensen, J. L. & Ørntoft, T. F. Normalization of real-time quantitative reverse transcription-PCR data: a model-based variance estimation approach to identify genes suited for normalization, applied to bladder and colon cancer data sets. *Cancer Res.* **64**, 5245–5250 (2004).

71. Kern, F. *et al.* miEAA 2.0: integrating multi-species microRNA enrichment analysis and workflow management systems. *Nucleic Acids Res.* **48**, W521–W528 (2020).

72. miRTarBase update 2022: an informative resource for experimentally validated miRNA-target interactions - PubMed. https://pubmed.ncbi.nlm.nih.gov/34850920/.

73. Milacic, M. *et al.* The Reactome Pathway Knowledgebase 2024. *Nucleic Acids Res.* **52**, D672–D678 (2024).

74. Joint Research Centre (European Commission) *et al. The Certification of Water-Soluble Ions in a Fine Dust (PM2,5-like) Material: ERM CZ110 : Certification Report*. (Publications Office of the European Union, 2020).

75. Schantz, M. M. *et al.* Development of two fine particulate matter standard reference materials (<4 μm and <10 μm) for the determination of organic and inorganic constituents. *Anal. Bioanal. Chem.* **408**, 4257–4266 (2016).

76. Rovelli, S. *et al.* How to obtain large amounts of location- and time-specific PM2.5 with homogeneous mass and composition? A possible approach, from particulate collection to chemical characterization. *Atmospheric Pollut. Res.* **12**, 101193 (2021).

77. Liebner, S. *et al.* Wnt/beta-catenin signaling controls development of the blood-brain barrier. *J. Cell Biol.* **183**, 409–417 (2008).

78. Czupalla, C. J., Liebner, S. & Devraj, K. In vitro models of the blood-brain barrier. *Methods Mol. Biol. Clifton NJ* **1135**, 415–437 (2014).

79. Han, D., Dong, X., Zheng, D. & Nao, J. MiR-124 and the Underlying Therapeutic Promise of Neurodegenerative Disorders. *Front. Pharmacol.* **10**, 1555 (2019).

80. Birtele, M. *et al.* Dual modulation of neuron-specific microRNAs and the REST complex promotes functional maturation of human adult induced neurons. *FEBS Lett.* **593**, 3370–3380 (2019).

81. Ludwig, N. *et al.* Distribution of miRNA expression across human tissues. *Nucleic Acids Res.* **44**, 3865–3877 (2016).

82. Kavakiotis, I., Alexiou, A., Tastsoglou, S., Vlachos, I. S. & Hatzigeorgiou, A. G. DIANA-miTED: a microRNA tissue expression database. *Nucleic Acids Res.* **50**, D1055–D1061 (2022).

83. Schopman, N. C. T., Heynen, S., Haasnoot, J. & Berkhout, B. A miRNA-tRNA mix-up: tRNA origin of proposed miRNA. *RNA Biol.* **7**, 573–576 (2010).

84. Li, N., Hao, M., Phalen, R. F., Hinds, W. C. & Nel, A. E. Particulate air pollutants and asthma. A paradigm for the role of oxidative stress in PM-induced adverse health effects. *Clin. Immunol. Orlando Fla* **109**, 250–265 (2003).

85. Shi, M. *et al.* Plasma exosomal α-synuclein is likely CNS-derived and increased in Parkinson's disease. *Acta Neuropathol. (Berl.)* **128**, 639–650 (2014).

86. Fiandaca, M. S. *et al.* Identification of preclinical Alzheimer's disease by a profile of pathogenic proteins in neurally derived blood exosomes: A case-control study. *Alzheimers Dement.* **11**, 600-607.e1 (2015).

87. Saeedi, S. *et al.* Neuron-derived extracellular vesicles enriched from plasma show altered size and miRNA cargo as a function of antidepressant drug response. *Mol. Psychiatry* **26**, 7417–7424 (2021).

88. Auber, M. & Svenningsen, P. An estimate of extracellular vesicle secretion rates of human blood cells. *J. Extracell. Biol.* **1**, e46 (2022).

89. You, Y. *et al.* ATP1A3 as a target for isolating neuron-specific extracellular vesicles from human brain and biofluids. *Sci. Adv.* **9**, eadi3647.

90. Norman, M. *et al.* L1CAM is not associated with extracellular vesicles in human cerebrospinal fluid or plasma. *Nat. Methods* **18**, 631–634 (2021).

91. Gomes, D. E. & Witwer, K. W. L1CAM-associated extracellular vesicles: A systematic review of nomenclature, sources, separation, and characterization. *J. Extracell. Biol.* **1**, e35 (2022).

92. Gu, D. *et al.* Elevated matrix metalloproteinase-9 levels in neuronal extracellular vesicles in Alzheimer's disease. *Ann. Clin. Transl. Neurol.* **7**, 1681–1691 (2020).

93. Yan, S. *et al.* Neuronally Derived Extracellular Vesicle α-Synuclein as a Serum Biomarker for Individuals at Risk of Developing Parkinson Disease. *JAMA Neurol.* **81**, 59–68 (2024).

94. Bhargava, P. *et al.* Synaptic and Complement Markers in Extracellular Vesicles in Multiple Sclerosis. *Mult. Scler. Houndmills Basingstoke Engl.* **27**, 509–518 (2021).

95. Banack, S. A., Dunlop, R. A., Stommel, E. W., Mehta, P. & Cox, P. A. miRNA extracted from extracellular vesicles is a robust biomarker of amyotrophic lateral sclerosis. *J. Neurol. Sci.* **442**, 120396 (2022).

96. Goetzl, E. J., Srihari, V. H., Mustapic, M., Kapogiannis, D. & Heninger, G. R. Abnormal levels of mitochondrial Ca2+ channel proteins in plasma neuron-derived extracellular vesicles of early schizophrenia. *FASEB J. Off. Publ. Fed. Am. Soc. Exp. Biol.* **36**, e22466 (2022).

97. Nasca, C. *et al.* Insulin receptor substrate in brain-enriched exosomes in subjects with major depression: on the path of creation of biosignatures of central insulin resistance. *Mol. Psychiatry* (2020) doi:10.1038/s41380-020-0804-7.

98. Burrows, K. *et al.* Exploring the role of neuronal-enriched extracellular vesicle miR-93 and interoception in major depressive disorder. *Transl. Psychiatry* **14**, 199 (2024).

99. Dunlop, R. A., Banack, S. A. & Cox, P. A. L1CAM immunocapture generates a unique extracellular vesicle population with a reproducible miRNA fingerprint. *RNA Biol.* **20**, 140–148 (2023).

100. Ko, S. Y., Lee, W. & Naora, H. Harnessing microRNA-enriched extracellular vesicles for liquid biopsy. *Front. Mol. Biosci.* **11**, (2024).

101. Dahlmanns, M., Dahlmanns, J. K., Savaskan, N., Steiner, H.-H. & Yakubov, E. Glial Glutamate Transporter-Mediated Plasticity: System xc-/xCT/SLC7A11 and EAAT1/2 in Brain Diseases. *Front. Biosci. Landmark Ed.* **28**, 57 (2023).

102. Hernández Borrero, L. J. & El-Deiry, W. S. Tumor suppressor p53: Biology, signaling pathways, and therapeutic targeting. *Biochim. Biophys. Acta BBA - Rev. Cancer* **1876**, 188556 (2021).

103. Coppola, V. *et al.* The autophagic protein FYCO1 controls TNFRSF10/TRAIL receptor induced apoptosis and is inactivated by CASP8 (caspase 8). *Autophagy* **19**, 2733–2751 (2023).

104. Labbé, J. C. *et al.* The study of the determinants controlling Arpp19 phosphatase-inhibitory activity reveals an Arpp19/PP2A-B55 feedback loop. *Nat. Commun.* **12**, 3565 (2021).

105. Svedružić, Ž. M. Chapter 6 - Dnmt1: Structure and Function. in *Progress in Molecular Biology and Translational Science* (eds. Cheng, X. & Blumenthal, R. M.) vol. 101 221–254 (Academic Press, 2011).

106. Dai, M., Yan, L., Yu, H., Chen, C. & Xie, Y. TNFRSF10B is involved in motor dysfunction in Parkinson's disease by regulating exosomal α-synuclein secretion from microglia. *J. Chem. Neuroanat.* **129**, 102249 (2023).

107. Sullivan, P. F., Neale, M. C. & Kendler, K. S. Genetic epidemiology of major depression: review and meta-analysis. *Am. J. Psychiatry* **157**, 1552–1562 (2000).

108. Fava, M. & Kendler, K. S. Major depressive disorder. *Neuron* **28**, 335–341 (2000).

109. Andrabi, S. M. *et al.* Nitric Oxide: Physiological Functions, Delivery, and Biomedical Applications. *Adv. Sci. Weinh. Baden-Wurtt. Ger.* **10**, e2303259 (2023).

110. Thiel, V. E. & Audus, K. L. Nitric oxide and blood-brain barrier integrity. *Antioxid. Redox Signal.* **3**, 273–278 (2001).

111. Ashraf, N. S. *et al.* Role of exosomal miRNA-19a/19b and PTEN in brain tumor diagnosis. *Future Oncol. Lond. Engl.* **19**, 1563–1576 (2023).

112. Guzman, N. *et al.* Breast Cancer-Specific miR Signature Unique to Extracellular Vesicles Includes 'microRNA-like' tRNA Fragments. *Mol. Cancer Res. MCR* **13**, 891–901 (2015).

113. Pontis, F. *et al.* Circulating extracellular vesicles from individuals at high-risk of lung cancer induce pro-tumorigenic conversion of stromal cells through transfer of miR-126 and miR-320. *J. Exp. Clin. Cancer Res. CR* **40**, 237 (2021).

114. Petrova, T. *et al.* Topographic Distribution of miRNAs (miR-30a, miR-223, miR-let-7a, miR-let-7f, miR-451, and miR-486) in the Plasma Extracellular Vesicles. *Non-Coding RNA* **10**, 15 (2024).

115. Hubert, A. *et al.* The relationship between residential exposure to atmospheric pollution and circulating miRNA in adults living in an urban area in northern France. *Environ. Int.* **174**, 107913 (2023).

116. Al-Rawaf, H. A., Alghadir, A. H. & Gabr, S. A. Circulating microRNAs and Molecular Oxidative Stress in Older Adults with Neuroprogression Disorders. *Dis. Markers* **2021**, 4409212 (2021).

117. Ravnik-Glavač, M. & Glavač, D. Circulating RNAs as Potential Biomarkers in Amyotrophic Lateral Sclerosis. *Int. J. Mol. Sci.* **21**, 1714 (2020).

118. Villela, D. *et al.* Differential DNA Methylation of MicroRNA Genes in Temporal Cortex from Alzheimer's Disease Individuals. *Neural Plast.* **2016**, 2584940 (2016).

119. Kuang, W.-H., Dong, Z.-Q., Tian, L.-T. & Li, J. MicroRNA-451a, microRNA-34a-5p, and microRNA-221-3p as predictors of response to antidepressant treatment. *Braz. J. Med. Biol. Res.* **51**, e7212 (2018).

120. Hu, P. *et al.* MicroRNA-451a is a candidate biomarker and therapeutic target for major depressive disorder. *Gen. Psychiatry* **37**, e101291 (2024).

121. Ferrari, L. *et al.* Extracellular vesicles and their miRNA contents counterbalance the pro-inflammatory effect of air pollution during physiological pregnancy: A focus on Syncytin-1 positive vesicles. *Environ. Int.* **169**, (2022).

122. D'Amico, G. *et al.* Air Pollution: Role of Extracellular Vesicles-Derived Non-Coding RNAs in Environmental Stress Response. *Cells* **12**, 1498 (2023).

123. Rodosthenous, R. S. *et al.* Ambient particulate matter and microRNAs in extracellular vesicles: a pilot study of older individuals. *Part. Fibre Toxicol.* **13**, 13 (2016).

124. Li, X. *et al.* miR-19 family: A promising biomarker and therapeutic target in heart, vessels and neurons. *Life Sci.* **232**, 116651 (2019).

125. Mazzelli, M. *et al.* The Long-Term Effects of Early Life Stress on the Modulation of miR-19 Levels. *Front. Psychiatry* **11**, 389 (2020).

126. Cioanca, A. V. *et al.* Multiomic integration reveals neuronal-extracellular vesicle coordination of gliotic responses in degeneration. *J. Extracell. Vesicles* **12**, 12393 (2023).

127. Schell, G., Roy, B., Prall, K. & Dwivedi, Y. miR-218: A Stress-Responsive Epigenetic Modifier. *Non-Coding RNA* **8**, 55 (2022).

128. Pulcrano, S. *et al.* miR-218 Promotes Dopaminergic Differentiation and Controls Neuron Excitability and Neurotransmitter Release through the Regulation of a Synaptic-Related Genes Network. *J. Neurosci. Off. J. Soc. Neurosci.* **43**, 8104–8125 (2023).

129. Wan, Z. *et al.* miR-218-5p and miR-320a-5p as Biomarkers for Brain Disorders: Focus on the Major Depressive Disorder and Parkinson's Disease. *Mol. Neurobiol.* **60**, 5642–5654 (2023).

130. Antoniou, A. *et al.* Neuronal extracellular vesicles and associated microRNAs induce circuit connectivity downstream BDNF. *Cell Rep.* **42**, 112063 (2023).

131. Kolshus, E. *et al.* Peripheral blood microRNA and VEGFA mRNA changes following electroconvulsive therapy: implications for psychotic depression. *Acta Psychiatr. Scand.* **136**, 594–606 (2017).

132. Xu, Y.-Y., Xia, Q.-H., Xia, Q.-R., Zhang, X.-L. & Liang, J. MicroRNA-Based Biomarkers in the Diagnosis and Monitoring of Therapeutic Response in Patients with Depression. *Neuropsychiatr. Dis. Treat.* **15**, 3583–3597 (2019).

133. Stoddart, M. J. Cell viability assays: introduction. *Methods Mol. Biol. Clifton NJ* **740**, 1–6 (2011).

134. Yuan, Y. *et al. In vitro* toxicity evaluation of heavy metals in urban air particulate matter on human lung epithelial cells. *Sci. Total Environ.* **678**, 301–308 (2019).

135. Balali-Mood, M., Naseri, K., Tahergorabi, Z., Khazdair, M. R. & Sadeghi, M. Toxic Mechanisms of Five Heavy Metals: Mercury, Lead, Chromium, Cadmium, and Arsenic. *Front. Pharmacol.* **12**, (2021).

136. Lee, D. C. *et al.* Eupatilin Inhibits Reactive Oxygen Species Generation via Akt/NF-κB/MAPK Signaling Pathways in Particulate Matter-Exposed Human Bronchial Epithelial Cells. *Toxics* **9**, 38 (2021).

137. Li, N., Hao, M., Phalen, R. F., Hinds, W. C. & Nel, A. E. Particulate air pollutants and asthma: A paradigm for the role of oxidative stress in PM-induced adverse health effects. *Clin. Immunol.* **109**, 250–265 (2003).

138. Liu, Q. *et al.* circRNAs deregulation in exosomes derived from BEAS-2B cells is associated with vascular stiffness induced by PM2.5. *J. Environ. Sci. China* **137**, 527–539 (2024).

139. Liu, F. *et al.* Macrophages treated with particulate matter PM2.5 induce selective neurotoxicity through glutaminase-mediated glutamate generation. *J. Neurochem.* **134**, 315–326 (2015).

140. Rota, F. *et al.* Blood-derived extracellular vesicles isolated from healthy donors exposed to air pollution modulate in vitro endothelial cells behavior. *Sci. Rep.* **10**, 20138 (2020).

141. Calderón-Garcidueñas, L. *et al.* Environmental Nanoparticles Reach Human Fetal Brains. *Biomedicines* **10**, 410 (2022).

ACKNOWLEDGEMENTS

When I started my Ph.D., I expected that research was mostly based on designing and carrying out experiments, mastering new lab techniques, and writing papers. I was wrong! Besides this, and perhaps most importantly, I learned to deal with a multitude of problems, to adapt to the unexpected, to manage stressful situations, but also to ask for help when necessary, to confidently share my opinions, and to stand up for my ideas. Regardless of what my future career will be, I will never regret having embarked on this amazing journey.

First of all, I would like to thank Prof. Michele Carugno, for being a great supervisor, always supportive and ready to help.

Special thanks also go to Prof. Valentina Bollati, for sharing her enthusiasm for research, and for consistently offering her unique (and sometimes unconventional) perspectives.

I would also like to extend my gratitude to all the members of the EPIGET lab, especially Rachele, Eva and Laura, who tenaciously assisted me in carrying out the experiments, as well as Elisa, Simona and Davide for their contribution to statistical and bioinformatic analyses. My thanks also go to Prof. Angela Pesatori and Prof. Massimiliano Buoli, for sharing their immense expertise in epidemiology and psychiatry, and to Prof. Andrea Cattaneo for his support on the PM side.

I cannot forget to thank Dr. Stefan Momma and Dr. Stefan Liebner, for welcoming me into their labs, allowing me to broaden my research perspectives and to have a taste of the “working and living abroad” full package of experiences.

Last but certainly not least, a heartfelt thanks to my family, all my friends (in Italy and Germany), and Luiz (now “biologist *ad honorem*”) for the great times together and for always supporting me through hardships.